Title: Functional genomics of trypanotolerant and trypanosusceptible cattle infected with *Trypanosoma congolense* across multiple time points and tissues

Short title: Functional genomics of trypanotolerant and trypanosusceptible cattle

Authors and Affiliations: Gillian P. McHugo[1], James A. Ward[1], John A. Browne[1], Grace M. O'Gorman[2], Kieran G. Meade[1,3], Emmeline W. Hill[1], Thomas J. Hall[1], David E. MacHugh[1,3,4*]

[1] UCD School of Agriculture and Food Science, University College Dublin, Belfield, Dublin, Ireland.

[2] UK Agri-Tech Centre, Innovation Centre, York Science Park, York, UK.

[3] UCD Conway Institute of Biomolecular and Biomedical Research, University College Dublin, Dublin, Ireland.

[4] UCD One Health Centre, University College Dublin, Dublin, Ireland.

* Corresponding author

Email: david.machugh@ucd.ie

Abstract

Human African trypanosomiasis (HAT), or sleeping sickness, is a neglected tropical disease caused by infection with trypanosome parasites (*Trypanosoma* spp.). These are transmitted by infected tsetse flies (*Glossina* spp.) and cause a similar disease in animals, known as African animal trypanosomiasis (AAT). AAT is one of the largest constraints to livestock production in sub-Saharan Africa and causes a financial burden of approximately $4.5 billion annually. Some African *Bos taurus* cattle populations have an important evolutionary adaptation known as trypanotolerance, a genetically determined tolerance of infection by trypanosome parasites (*Trypanosoma* spp.). Trypanotolerant African *B. taurus* N'Dama and trypanosusceptible *Bos indicus* Boran cattle responded in largely similar ways during trypanosome infection when gene expression was examined using blood, liver, lymph node, and spleen samples with peaks and troughs of gene expression differences following the cyclic pattern of parasitaemia exhibited during trypanosome infection. However, differences in response to infection between the two breeds were reflected in differential expression of genes related to the immune system such as those encoding antimicrobial peptides and cytokines, including, for example, the antimicrobial peptide encoding genes *LEAP2*, *CATHL3*, *DEFB4A*, and *S100A7* and the cytokine genes *CCL20*, *CXCL11*, *CXCL13*, *CXCL16*, *CXCL17*, *IL33*, and *TNFSF13B*. In addition, transcriptional profiling of peripheral blood identified expression differences in genes relating to coagulation and iron homeostasis, which supports the hypothesis that the dual control of parasitaemia and the anaemia resulting from the innate immune response to trypanosome parasites is key to trypanotolerance and provide new insights into the molecular mechanisms underlying this phenomenon.

Author Summary

Trypanosome parasites are transmitted by infected tsetse flies and cause the neglected tropical disease human African trypanosomiasis (HAT) and the similar African animal trypanosomiasis (AAT), which is one of the largest impediments to livestock production in sub-Saharan Africa. Taurine (*Bos taurus*) and indicine (*Bos indicus*) cattle shared a common ancestor more than 150,000 years ago, and in the intervening period significant genomic differences have evolved between the two groups. Importantly, several African *B. taurus* populations have evolved an adaptation known as trypanotolerance, a genetically determined tolerance of infection by trypanosome parasites. Trypanotolerant African taurine and trypanosusceptible indicine cattle responded in largely similar ways during trypanosome infection when gene expression was examined using blood, liver, lymph node, and spleen samples with peaks and troughs of gene expression differences following the cyclic pattern of the number of trypanosome parasites in the blood. Transcriptional profiling of these tissues highlighted genes related to the multiple facets of the immune system; notably, for peripheral blood, differences observed for genes relating to coagulation and iron homeostasis support the existing hypothesis that control of both parasite number and anaemia is an important feature of the trypanotolerance trait and provide new insights into the molecular mechanisms underlying this phenomenon.

54 # Introduction

55 Trypanosomiasis is prevalent in humid and semi-humid regions of Africa and is a wasting
56 disease caused by parasitic protozoa of the genus *Trypanosoma* which are transmitted by biting
57 insect vectors such as tsetse flies (*Glossina* spp.) [1]. Human African trypanosomiasis (HAT),
58 caused by *T. brucei gambiense* or *T. brucei rhodesiense* infection, is also known as sleeping
59 sickness and is classed as a neglected tropical disease (NTD) by the World Health Organisation
60 [2]. Trypanosomes also infect animals and cause particularly severe disease in domesticated
61 animals—African animal trypanosomiasis (AAT)—for which the symptoms, as in HAT,
62 include fever, severe weight loss, and anaemia [1, 3, 4]. As the disease progresses, animals
63 weaken and become paralysed and unfit for work [1]. AAT is caused by a wider range of
64 trypanosome parasites, most commonly *T. congolense, T. vivax*, and *T. brucei* ssp., although
65 the prevalence and distribution of trypanosome species varies and co-infections are possible [5,
66 6]. In addition, domestic animals can also be infected with the human-infective trypanosome
67 species, for which they act as a reservoir [5, 7].

68 Animal models, including mice, have long been used to study human-infective
69 trypanosomes leading to important insights into host-trypanosome interactions [8-10]. The
70 usefulness of these animal models has been improved by the differential host tolerance of, or
71 susceptibility to, trypanosome infection that has been found between different cattle breeds,
72 mouse strains, and human populations, although the underlying genes differ between host
73 species [11-14]. Conversely, while it is much less common, humans may also be infected with
74 trypanosome species more frequently found in animals, resulting in atypical human
75 trypanosomiasis [5, 15]. With climate change and increasing globalisation there is growing
76 concern that this atypical human trypanosomiasis may represent an emerging neglected
77 zoonotic disease that underscores the importance of a One Health approach to both human and
78 animal trypanosomiasis [16].Trypanosomiasis has a limiting effect on sub-Saharan livestock
79 production, because even with application of trypanocidal drugs, the susceptibility of most

80 cattle to trypanosomiasis makes production economically unsustainable in many regions on the
81 African continent [17].

82 Cattle are significant components of rural economies and livelihoods in Africa. They
83 provide milk, meat, fertiliser and traction and represent mobile assets that serve as a financial
84 buffer for poor families, particularly for pastoralists and women [18, 19]. There are
85 approximately 150 breeds of indigenous cattle in sub-Saharan Africa and African cattle
86 represent a complex mosaic of African *Bos taurus*, European *B. taurus*, *B. indicus*, and various
87 hybrid populations [20-22]. African cattle form a gradient of *B. taurus* and *B. indicus* ancestry
88 across the continent [20]. This is a result of multiple domestications and the subsequent spread
89 of distinct populations of cattle across Africa [23]. The spread of agriculture and livestock
90 herding has also shaped African human genetics and linguistic variation, illustrating the
91 importance of domesticated species in influencing recent human evolution [24, 25]. Zebu or
92 indicine breeds, which have primarily *B. indicus* ancestry, are favoured by many farmers due
93 to their larger size and higher production yields [26]. However, cattle populations in West
94 Africa tend to have higher level of taurine (*B. taurus*) ancestry [20, 27]. This is because some
95 indigenous *B. taurus* breeds have an advantage in western sub-Saharan Africa due to their
96 tolerance of trypanosomes, a trait termed "trypanotolerance" [26, 28]. These cattle exhibit a
97 greater ability to control parasitaemia and anaemia, making them more productive than *B.*
98 *indicus* cattle or other *B. taurus* breeds in areas infested with tsetse flies and trypanosomes [26,
99 29]. These trypanotolerant breeds, which include the longhorn N'Dama and shorthorn Baoule,
100 Lagune, and Somba breeds, are therefore an important genetic resource as they are uniquely
101 suited to livestock production in these areas [30, 31]. Trypanotolerant breeds only make up 6%
102 of the total cattle population of Africa and but represent 17% of the cattle in the tsetse infested
103 areas [32]. Although trypanotolerance is a valuable trait in these areas, trypanotolerant breeds
104 such as the N'Dama, are not more widely used because of their relatively inferior production

105 characteristics, unpredictable temperament and smaller size, which make them unsuitable for
106 draft purposes [32, 33].

107 Trypanotolerance has been shown to be a heritable trait, although there is variability in
108 tolerance between animals within breeds [13, 29, 34, 35]. Trypanotolerant breeds are also less
109 susceptible to other infectious diseases such as helminthiasis, ticks and tick-borne-diseases and
110 genes associated with the immune response have been found to be under selection in west
111 African cattle populations [36, 37]. Trypanotolerant and trypanosusceptible breeds have been
112 shown to vary in their immune responses and exhibit gene expression differences in various
113 tissues at key points during infection after infection with trypanosomes [33, 38-42]. They also
114 show differences in ability to control anaemia over two years [43]. There are also *B. taurus*/*B.*
115 *indicus* hybrid breeds that have been observed to be trypanotolerant [44]. However,
116 trypanotolerant breeds with high levels of African *B. taurus* ancestry are better able to control
117 anaemia while hybrid animals exhibit intermediate levels of control when compared to
118 susceptible *B. indicus* breeds [45]. The genes, genomic regulatory elements (GREs), and
119 genomic regulatory networks (GRNs) underpinning trypanotolerance remain largely unknown,
120 although several candidate genes and regulatory mechanisms have been suggested based on
121 population genomics and functional genomics studies [33, 40, 42, 43, 46-49]. It has been
122 proposed that a better understanding of the trypanotolerance trait will facilitate genome-
123 informed breeding programmes that could also leverage transgenesis to enhance the trait,
124 thereby increasing the productivity of livestock production in sub-Saharan Africa [26, 33].

125 In this study we analysed Affymetrix® Bovine Genome Array gene expression data across
126 multiple tissues from trypanotolerant N'Dama and trypanosusceptible Boran cattle that had
127 been infected with *T. congolense* across an infection time course [33, 40, 41]. We used
128 previously published data from liver, lymph node, and spleen tissue samples and combined
129 these data with new peripheral blood mononuclear cell (PBMC) data from the same animals.

130 Differentially expressed genes (DEGs) were detected across the infection time course for each
131 breed and between the two breeds for each time point. The sets of DEGs were then used for
132 functional enrichment analyses focused on gene ontology (GO) to catalogue and interrogate
133 biological processes associated with disease pathogenesis and trypanotolerance.

Materials and methods

Data sources

New microarray gene expression data

Affymetrix® Bovine Genome Array data sets were generated for 40 peripheral blood mononuclear cell (PBMC) samples from 10 African cattle (5 trypanotolerant N'Dama and 5 trypanosusceptible Boran) collected at four time points for a *T. congolense* infection experiment performed in 2003 [39-41]. The cattle, all female and aged between 19–28 months, were reared together at the International Livestock Research Institute (ILRI) ranch at Kapiti Plains Estate, Kenya which is located in an area free from tsetse flies and trypanosomiasis [41]. The cattle were experimentally infected with the *T. congolense* clone IL1180 [50, 51] delivered via the bites of eight infected tsetse flies (*Glossina morsitans morsitans*) [52, 53] at the ILRI laboratories in Nairobi, Kenya. The flies were allowed to feed on the shaved flanks of the animals until engorgement. The infections were carried out in three batches which took place two weeks apart and were confirmed by microscopy. Parasitaemia and anaemia measured by packed cell volume (PCV) were monitored throughout the course of the infection [41].

Peripheral blood (200 ml) was collected in heparinised syringes before infection and at 14, 25, and 34 days post-infection (DPI), these time points were selected to align with the first wave of parasitaemia [41]. This animal work was completed prior to the requirement for formal Institutional Permission in Ireland, which is based on European Union Directive 2010/63/EU; however, all animal procedures were approved by the Institutional Animal Use and Care (IAUC) Committee of ILRI in accordance with the UK Animals (Scientific Procedures) Act 1986 and all efforts were made to ensure high welfare standards and ethical handling of animal subjects.

Peripheral blood mononuclear cell (PBMC) samples were isolated from the blood samples with Percoll™ gradients (GE Healthcare, Buckinghamshire, UK) and total RNA was

159 extracted from the PBMCs in TriReagent (Molecular Research Center, Inc., Cincinnati, OH,
160 USA) and the RNA samples were then DNase-treated and purified using an RNeasy mini kit
161 (Qiagen Ltd., Crawley, UK). RNA quality and quantity was assessed using the 18S/28S ratio
162 and RNA integrity number (RIN) on an Agilent Bioanalyzer with the RNA 6000 Nano
163 LabChip® kit (Agilent Technologies, Inc., Santa Clara, CA, USA). Following this, cDNA
164 labelling, hybridisation and scanning for the microarray experiments were performed by Almac
165 Diagnostic Services (Craigavon, Northern Ireland) using a one-cycle amplification/labelling
166 protocol. Gene expression data in the form of cell intensity files (.CEL) were generated using
167 the Affymetrix GeneChip® Operating Software (GCOS) package. The Affymetrix® GeneChip®
168 Bovine Genome Array data sets generated for this study have been deposited in the European
169 Molecular Biology Laboratory European Bioinformatics Institute ArrayExpress data repository
170 under accession number E-MTAB-14517 (temporary manuscript reviewer link:
171 https://www.ebi.ac.uk/biostudies/arrayexpress/studies/E-MTAB-14517?key=b9fd37fb-644d-
172 442b-b443-53506a43a8df).

173 *Previously published microarray gene expression data*

174 Additional Affymetrix® Bovine Genome Array data sets were obtained from a published
175 study using solid tissues samples from the same animal infection time course [33] resulting in
176 a total of 220 biological samples across 12 infection time points and four tissues (for both
177 N'Dama and Boran) before filtering (**Table 1**). **Fig 1** illustrates the experimental design and
178 study workflow. The computer code required to repeat and reproduce the analyses is available
179 at doi.org/10.5281/zenodo.11502109.

180 **Table 1.** Days post infection, tissues, numbers of N'Dama (NDAM) and Boran (BORA)
181 samples, and sources of microarray data used in this study before and after sample filtering.

Days post infection	Tissue	No. NDAM samples pre-filtering	No. BORA samples pre-filtering	No. NDAM samples post-filtering	No. BORA samples post-filtering	Source*
0	Blood (PBMC)	5	5	5	5	a
0	Liver	20	20	19	18	b
0	Lymph node	5	5	5	4	b
0	Spleen	5	5	5	4	b
12	Liver	5	5	5	5	b
14	Blood (PBMC)	5	5	5	5	a
15	Liver	5	5	5	5	b
18	Liver	5	5	5	5	b
21	Liver	5	5	5	5	b
21	Lymph node	5	5	4	5	b
21	Spleen	5	5	5	5	b
25	Blood (PBMC)	5	5	5	5	a
26	Liver	5	5	3	5	b
29	Liver	5	5	5	5	b
32	Liver	5	5	5	5	b
34	Blood (PBMC)	5	5	5	5	a
35	Liver	5	5	5	5	b
35	Lymph node	5	5	4	5	b
35	Spleen	5	5	5	5	b
Population total		110	110	105	106	
	Total	220		211		

182 *a this study, b [33].

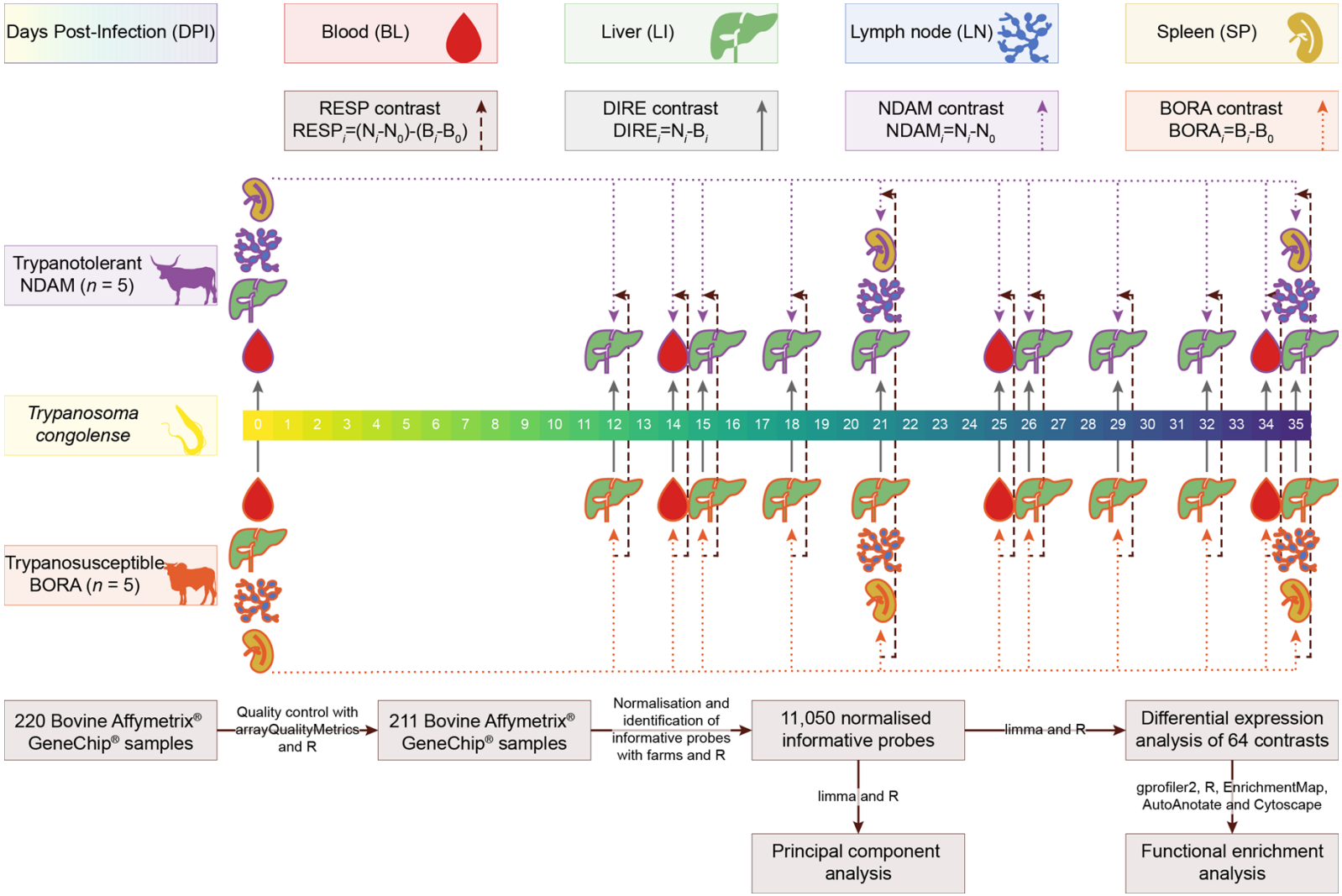

Fig 1. Diagram showing the experimental design and study workflow. Trypanosome image by Matus Valach and cattle images by Tracy A. Heath and T. Michael Keesey via phylopic.org and tissue images via healthicons.org. Colours were generated from the khroma (v. 1.10.0) [54] and viridis (v. 0.6.3) [55] R packages.

Data filtering and normalisation

Quality control with log transformation was performed using affy (v. 1.80.0) [56], Biobase (v. 2.62.0) [57], and arrayQualityMetrics (v. 3.58.0) [58] with R (v. 4.3.2) [59]. As in previous microarray studies, any individual samples that were identified as outliers in two or more quality control tests were discarded from the analysis [60]. Normalisation was performed using farms (v. 1.25.0) [61] with R (v. 4.3.2).

The intensity of expression for each sample was visualised both with the raw data and after normalisation using affy (v. 1.80.0), Biobase (v. 2.62.0), dplyr (v. 1.1.2) [62], ggh4x (v. 0.2.4) [63], ggplot2 (v. 3.4.2) [64], ggtext (v. 0.1.2) [65], magrittr (v. 2.0.3) [66], readr (v. 2.1.4) [67], reshape2 (v. 1.4.4) [68], and stringr (v. 1.5.0) [69] with R (v. 4.3.2). Colours were generated from khroma (v. 1.10.0) [54] and viridis (v. 0.6.3) [55]. Informative probe sets were identified and extracted using farms (v. 1.25.0) with R (v. 4.3.2).

Principal component analysis

Principal component analysis (PCA) was performed using limma (v. 3.58.1) [70] with R (v. 4.3.2). The results were visualised using dplyr (v. 1.1.2), ggplot2 (v. 3.4.2), patchwork (v. 1.2.0) [71], and stringr (v. 1.5.0), with R (v. 4.3.2). Colours were generated from khroma (v. 1.10.0) and viridis (v. 0.6.3).

Differential expression analysis

Differential expression analysis was performed using limma (v. 3.58.1) [70] with R (v. 4.3.2). The correlation between samples from the same animal was estimated and included in the linear model [70, 72]. The contrast matrix contained 64 contrasts across the two populations, four tissues and 12 time points which included direct (DIRE) contrasts to identify changes in expression in the N'Dama samples relative to the Boran samples ($DIRE_i = N_i - B_i$, where N represents the N'Dama population and B represents the Boran population), N'Dama (NDAM) and Boran (BORA) contrasts to identify changes in expression within the populations relative

212 to time 0 ($NDAM_i = N_i - N_0$; $BORA_i = B_i - B_0$) and response (RESP) contrasts to identify
213 changes in expression over time in the N'Dama samples relative to the Boran ($RESP_i = [N_i -$
214 $N_0] - [B_i - B_0]$) (**Fig 1**, **Table S1**) [33]. Moderated *t*-statistics, moderated *F*-statistic, and log-
215 odds of differential expression were calculated for the informative probe sets by empirical
216 Bayes moderation of the standard errors towards a global value [70, 73]. Global Benjamini-
217 Hochberg correction for multiple testing was applied across all contrasts [70, 74]. Probe sets
218 with an adjusted *P*-value of ≤ 0.05 (B-H $P_{adj.} \leq 0.05$) were determined to be significantly
219 differentially expressed [70]. The microarray probe sets were converted to genes using
220 gprofiler2 (v. 0.2.2) [75] with R (v. 4.3.2).

221 The results of the differential expression analysis were visualised using ComplexUpset
222 (v. 1.3.3) [76], dplyr (v. 1.1.2), ggh4x (v. 0.2.4), ggplot2 (v. 3.4.2), ggrepel (v. 0.9.3) [77],
223 patchwork (v. 1.2.0), readr (v. 2.1.4), rlang (v. 1.1.1) [78], stringr (v. 1.5.0), and tidyr (v 1.3.0)
224 [79] with R (v. 4.3.2). Colours were generated from khroma (v. 1.10.0) and viridis (v. 0.6.3).

225 Functional enrichment analysis

226 Functional enrichment was performed and visualised using dplyr (v. 1.1.2), ggh4x (v.
227 0.2.4), ggplot2 (v. 3.4.2), ggrepel (v. 0.9.3), gprofiler2 (v. 0.2.2), magick (v. 2.8.1) [80] with
228 ImageMagick (v. 6.9.12.96) [81], magrittr (v. 2.0.3), purrr (v. 1.0.1) [82], readr (v. 2.1.4), rlang
229 (v. 1.1.1), scales (v. 1.2.1) [83], and stringr (v. 1.5.0) with R (v. 4.3.2). Colours were generated
230 from khroma (v. 1.10.0) and viridis (v. 0.6.3). The background set was the set of informative
231 probe sets with valid Ensembl IDs. The query sets included those that were significantly
232 differentially expression (adjusted *P*-value ≤ 0.05) for each of the 64 contrasts. The analysis
233 was restricted to Gene Ontology (GO) terms and driver GO terms were highlighted. Generic
234 Enrichment Map (GEM) files were generated and used as input for EnrichmentMap (v. 3.3.6)
235 [84] with Cytoscape (v. 3.8.0) [75, 85, 86]. AutoAnotate (v. 1.3.5) [87] was used to create
236 clusters of GO terms with genes in common with clusterMaker2 (v. 2.0) [88] and annotate them

237 with appropriate names using WordCloud (v. 3.1.4) [89]. The yFiles Layout Algorithms (v.
238 1.1.3) method [90] was used to remove overlaps in the networks.

Results

Data filtering and normalisation

Nine samples were indicated as outliers by two or more of the quality control tests and were therefore removed, leaving 211 samples for analysis (**Fig S1**, **Table 1**). After normalisation the data were filtered to retain only informative probe sets, which resulted in a data set of 11,050 probe sets or 45.89% of the initial 24,128 probe sets.

Principal component analysis

Based on the top ten principal components (PCs), the first PC explained 82.86% of the total variation in the data for PC1–10 and separated the liver from the blood, lymph node, and spleen samples (**Fig 2**). The second PC explained a further 9.10% of the total variation for PC1–10 and separated the blood from the lymph node and spleen samples (**Fig 2**). The third and fourth PCs explained 2.24% and 1.78% of the total variation for PC1–10, respectively, and separated the samples according to days post infection (dpi) while the fifth PC, which explained 1.32% of the total variation in the data for PC1–10 separated the lymph node and spleen samples (**Fig S2–S4**).

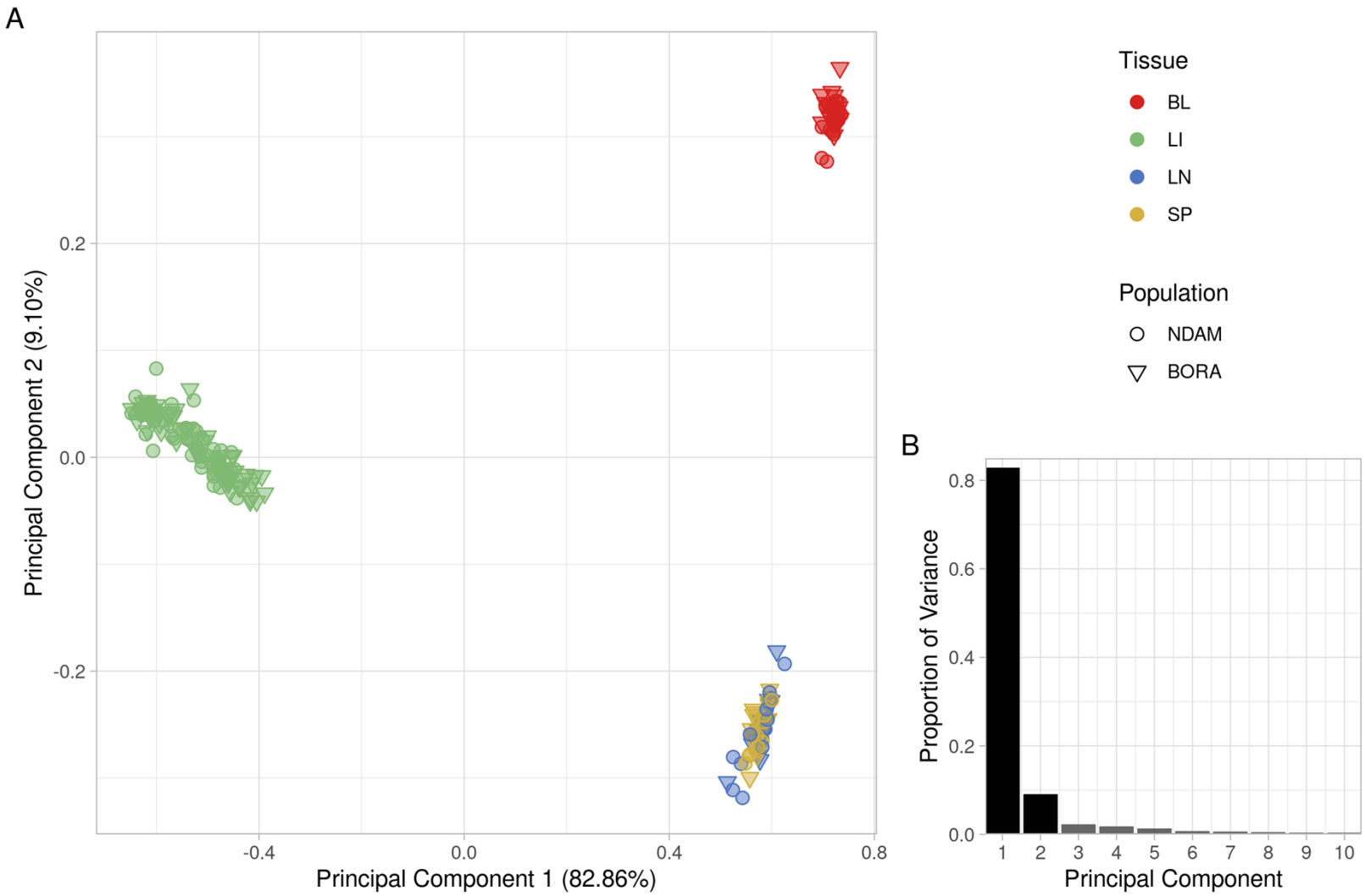

Fig 2. A. Principal component analysis (PCA) of the microarray data set with samples coloured according to tissue and with the shape indicating the population. The first two principal components (PC1 and PC2) are shown, and **B.** bar chart of proportion of variance of the top ten PCs.

Differential expression analysis

The results of the differential expression analysis are detailed in **Table S2** and the number of significant (B-H $P_{adj.} \leq 0.05$) differentially expressed genes (DEGs) generally increased over time across all contrast types and tissues until 21 dpi when they began to decrease slightly before rising again to their peak at 34 or 35 dpi (**Fig 3**, **S5–S8**). The highest numbers of significant DEGs were found in the N'Dama and Boran contrasts, followed by the direct contrasts (**Fig 3**). Within the response contrasts the highest number of significant DEGs were found in the lymph node samples at 35 dpi (**Fig 3**, **S5**) while the blood samples at 34 dpi had the highest number of significant DEGs in the direct contrasts (**Fig 3**, **S6**). The highest number of significant DEGs in the N'Dama and Boran contrasts were at 35 dpi in the lymph node and liver samples, respectively (**Fig 3**, **S7**, **S8**). The numbers of significant DEGs were generally higher in the N'Dama contrasts than in the Boran contrasts early in the time course (**Fig 3**).

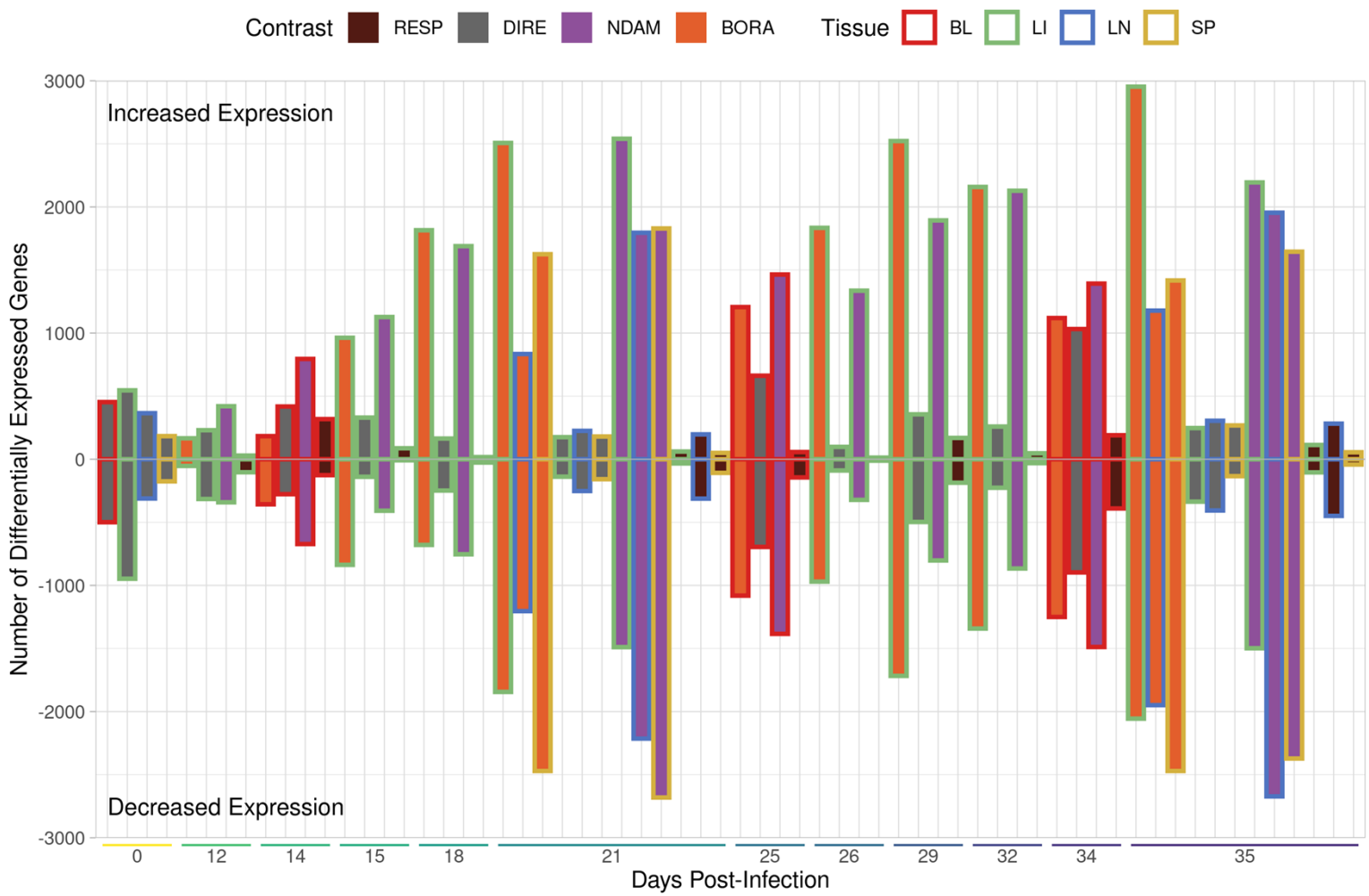

Fig 3. Bar chart showing the numbers of significant differentially expressed genes (DEGs) for all 64 contrasts (B-H $P_{adj.} \leq 0.05$). The extent of the bar above and below 0 on the *y*-axis indicates the numbers of significant DEGs with increased and decreased expression, respectively. The position on the *x*-axis indicates the number of days post infection (dpi). The bar colours represent the contrast type while the bar outline colours represent the tissue.

273 The N'Dama and Boran contrasts also had a higher number of significant DEGs in
274 common between them when overlaps among all 64 contrasts were examined (**Fig S9**). Within
275 the response and direct contrasts any overlaps in significant DEGs were generally confined to
276 those between samples from the same tissue type at different time points (**Fig S10**, **S11**) while
277 the N'Dama and Boran contrasts included more overlaps between tissues and time points (**Fig**
278 **S12**, **S13**).

279 There were also many overlaps when the top 10 most significant genes with increased
280 and decreased expression were examined for each of the contrasts (**Table 2**, **S3–S5**, **Fig 4**,
281 **S14–S27**). The set of 1,267 genes identified as being in the top 10 most significant for increased
282 or decreased expression for each of the 64 contrasts contained just 602 unique genes (**Table 2**,
283 **S3–S5**). Of these, 328 were in the top 10 most significant for only one contrast, with the
284 remaining 274 in the top 10 most significant for an average of 3.43 contrasts (**Table 2**, **S3–S5**).
285 The response contrasts had the most unique genes in the top 10 most significant with 129 of the
286 328 unique top genes, while the direct, N'Dama and Boran contrasts had 75, 58 and 66 unique
287 top genes, respectively (**Table 2**, **S3–S5**). The most common genes in the top 10 most
288 significant differentially expressed for all the contrasts included *TMSB10,* which was in the top
289 10 most significant genes for 16 of the 64 contrasts, followed by *CYRIB*, *PTPRC*, *SPI1*, and
290 *TTLL1*, which were in the top 10 most significant genes for 14 of the 64 contrasts (**Table 2**,
291 **S3–S5**). The *TMSB10* gene was in the top 10 most significant genes with increased expression
292 for the liver samples at all time points for the N'Dama and Boran contrasts (**Table S4**, **S5**). The
293 *CYRIB*, *PTPRC*, and *SPI1* genes showed similar patterns with the exclusion of 12 dpi (**Table**
294 **S4**, **S5**). *TTLL1* was in the top 10 most significant genes with increased expression in the blood
295 samples at 25 and 34 dpi and the liver samples at 18 dpi for the response contrasts (**Table 2**). It
296 was also in the top 10 most significant genes with increased expression for the blood samples
297 at 0, 14, 25, and 34 dpi, the liver samples at 18 dpi, and the lymph node and spleen samples at
298 0, 21, and 35 dpi for the direct contrasts (**Table S3**).

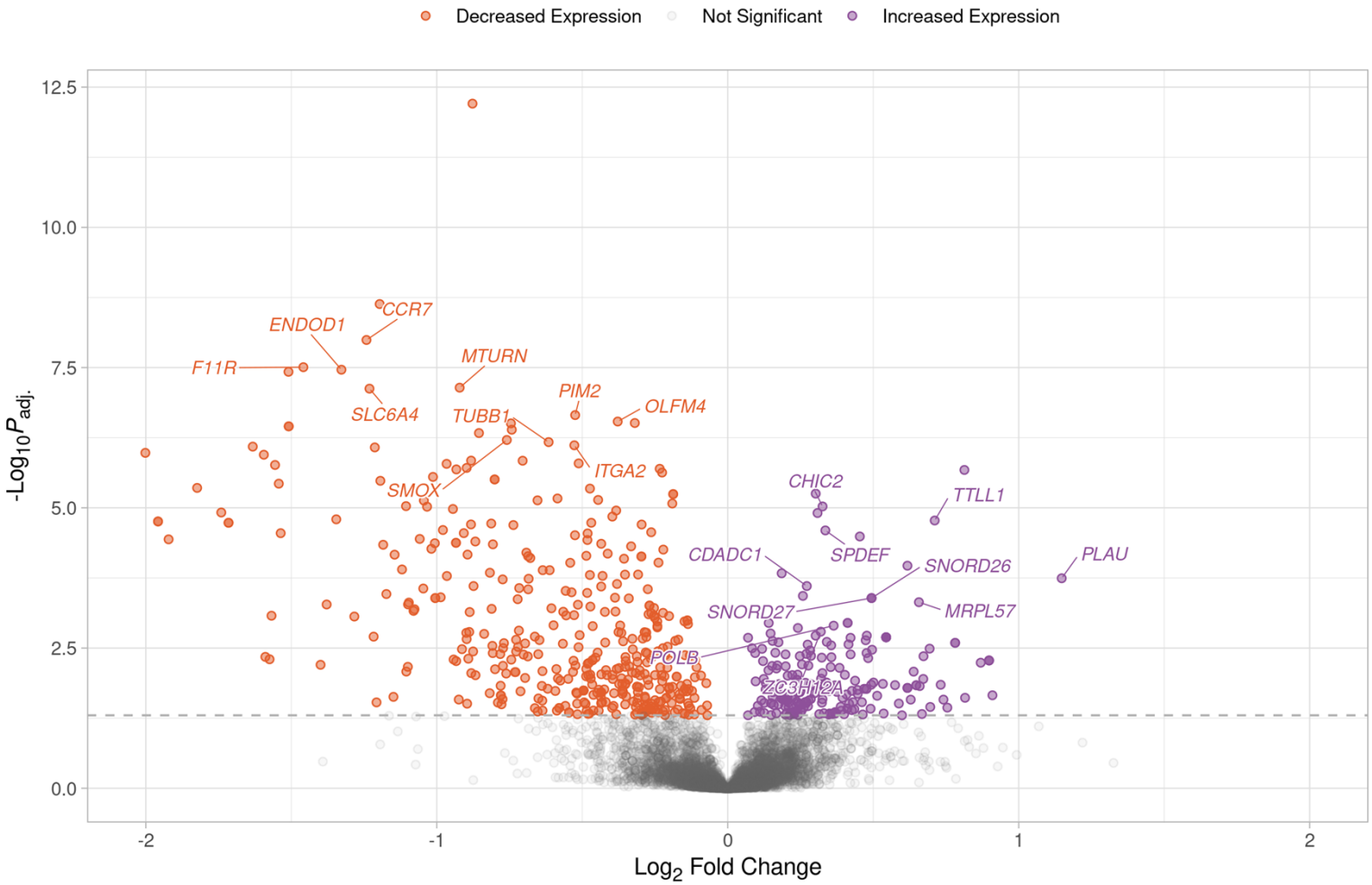

299

300 **Fig 4.** Volcano plot showing the results of the RESP contrast for the peripheral blood mononuclear cell (PBMC) samples at 34 days post infection (dpi).
301 Each data point represents a gene with the position on the *x*- and *y*-axes indicating the $\log_2$ fold change and $-\log_{10}P_{adj.}$, respectively. Genes above the
302 horizontal dashed line are significantly differentially expressed with the colours representing the change in expression. The top 10 most significant
303 genes for increased and decreased expression with gene symbols are labelled.

304 The most common genes in the top 10 most significant differentially expressed for the
305 response contrasts included *CYP4B1* and *RAB31,* which were in the top 10 most significant
306 genes for four of the 15 response contrasts, followed by *OLFM4*, *TMEM45B*, and *TTLL1,*
307 which were in the top 10 most significant genes for three of the 15 response contrasts (**Table**
308 **2**). For the response contrasts, *CYP4B1* was in the top 10 most significant genes with increased
309 expression for the spleen samples at 21 and 35 dpi and the top 10 most significant genes with
310 decreased expression for the lymph node samples at the same time point contrasts (**Table 2**).
311 It was also in the top 10 most significant genes with increased expression for the spleen samples
312 at 0 dpi and the top 10 most significant genes with decreased expression for the lymph node
313 samples at the same time point for the direct contrasts (**Table S3**). *RAB31* was only in the top
314 10 most significant genes with decreased expression for the liver samples at 26, 29, 32, and 35
315 dpi for the response contrasts (**Table 2**). For the response contrasts, *OLFM4* was in the top 10
316 most significant genes with decreased expression for the blood samples at 14, 25, and 34 dpi
317 (**Fig 4**, **Table 2**). It was also in the top 10 most significant genes with decreased expression for
318 the blood samples at 0 dpi for the direct contrasts, and at 14, 25, and 34 dpi for the N'Dama
319 contrasts (**Table S3**, **S4**). For the response contrasts, *TMEM45B* was in the top 10 most
320 significant genes with increased expression for the liver samples at 21, 26, and 29 dpi (**Table**
321 **2**). It was also in the top 10 most significant genes with decreased expression for the liver
322 samples at 0, 12, and 15 dpi for the direct contrasts (**Table S3**).

323 **Table 2.** Tissue, days post infection (dpi) and the top 10 most significant genes with increased
324 and decreased expression with valid gene symbols for the response contrasts.

Tissue	Days post infection	Most significant genes with increased expression
BL	14	*SRSF11, SNORD50B, CCAR1, RESF1, CLECL1P, KTN1, SENP6, KRR1, CCNL1, TRMT13*
BL	25	*RESF1, TTLL1, ADAMDEC1, COX6C, KLF5, S100A7, TLR6, CHIC2, ZNF318, RUM1*
BL	34	*CHIC2, TTLL1, SPDEF, PLAU, CDADC1, SNORD26, SNORD27, MRPL57, POLB, ZC3H12A*
LI	12	*IL18BP, FOXA3, CXCL11, DVL1, REG3A, CD40, BIRC3, SRGN, MAPK12, WARS1*
LI	15	*SGCB, RNF39, ITIH2, FBXO34, GNPAT, TCF20, bta-mir-2442, C8H9orf64, SCRN2, STAG2*
LI	18	*PCF11, TTLL1, PER1, NRG2, CIPC, MKNK2, BAG3, RPL22, ACTR8*
LI	21	*TMEM45B, RFTN1, UPF2, TCEA3, LTB, CPQ, PLIN5, ABCC5, OSGIN1, SMARCA2*
LI	26	*TMEM45B, CIDEA, ECT2L, CCDC191, RETSAT, PMVK, CA5A, ANP32A*
LI	29	*MAGI3, TMEM45B, NGFR, PPP2R5A, CBS, DPYS, MTMR4, UGT2B10, COLEC11, GSTA4*
LI	32	*SFRP2, APLNR, PLAC8B, CYP3A28, AAMDC, ST7L, MSMO1, SQLE, CES1, TCEA3*
LI	35	*CES1, RETSAT, CYP3A28, MTMR4, KCNK17, ABHD14B, ACP6, SYBU, ACY1, GCDH*
LN	21	*ALB, CXCL13, ATP6V0D2, EAF2, SUCLG1, ORC1, SNORA73, ECRG4, SKA2, TNFSF13B*
LN	35	*CCL20, RGS13, DEFB4A, MYB, ELL3, SNORA73, LXN, PLEKHF2, EED, SPAG5*
SP	21	*TRMT10B, CYP4B1, NXPH1, KCNA3, MDK, KIRREL2, PTGDS, FAM83D, PRR5L, LTB*
SP	35	*CYP4B1, MAB21L1, FAM83D, IKZF2, SNCA, PRR5L, RNASE4, RGS13, ZCCHC17, TARP*
Tissue	**Days post infection**	**Most significant genes with decreased expression**
BL	14	*OLFM4, PGA5, CDC42EP3, ORAI3, KAT7, VAT1L, PMF1, OASL, RAVER1, ICAM3*
BL	25	*SLC6A4, OLFM4, PGA5, SMOX, PRDM1, SLC9A6, PFKFB4, CCR7, MEIS1, F11R*
BL	34	*CCR7, ENDOD1, SLC6A4, PIM2, OLFM4, SMOX, TUBB1, ITGA2, DSTN, SLC40A1*
LI	12	*NUDT12, APOB, PLD1, MYO1B, IQGAP2, CRYZ, EPS8, MASP1, APC, CYP4V2*
LI	15	*MAPK6, TCIRG1, CXCL17, CUL1, XRN2*
LI	18	*MEP1B, SLC1A3, TJP2, OLR1, ACTG1, bta-mir-3533, IGFALS, NAE1, IMPA1, SNX6*
LI	21	*LEAP2, C15H11orf52, SLC25A25, ABHD10, ANGPTL8, LPAR6, KBTBD6, MTRF1, MFSD2A, ISG12(B)*
LI	26	*PAMR1, RAB31, VLDLR, GPLD1*

325 **Table 2 continued.**

Tissue	Days post infection	Most significant genes with decreased expression
LI	29	*PEG3, RAB31, JCHAIN, WWOX, OTULINL, DNMT1, OLR1, ACTG1, bta-mir-3533, PLTP*
LI	32	*MEP1B, SLC1A3, JCHAIN, RPSA, SNORA62, XRCC5, RAB31, LDHA, WWOX, CORO1B*
LI	35	*ANGPTL8, RAB31, LEAP2, ANGPTL4, VLDLR, PLOD2, BNIP3, GNL2, MTMR11, S100A8*
LN	21	*CLDN11, STAB1, CYP4B1, BRB, P2RX4, PROS1, KANK3, HYAL2, ELOVL7, COLEC12*
LN	35	*BRB, CYP4B1, STAB1, CLDN11, PROS1, HEPH, P2RX4, MAN1C1, C1QTNF5, SCARA5*
SP	21	*BMP2, FABP3, GRO1, THBS1, BCL10, F2RL2, CLDN1, SAMSN1, TLR4, ARL14EP*
SP	35	*NELL2, CD14, ITGA8, MUSTN1, RBP1, F2RL2, CXCL16, IL33, CATHL3, BMP2*

326

327 Functional enrichment analysis

328 GO terms related to regulation of the mitotic cell cycle were significantly enriched for
329 the genes with significantly increased expression in the blood and lymph node samples for the
330 response contrasts (**Fig 5**). The top driver GO terms for the blood samples included
331 *GO:0006396 RNA processing* and *GO:0005730 nucleolus* (**Fig S28**) while the top driver GO
332 terms for the lymph node samples included *GO:0007059 chromosome segregation*,
333 *GO:0005694 chromosome*, *GO:0006259 DNA metabolic process*, *GO:0006260 DNA*
334 *replication*, *GO:0051301 cell division*, *GO:0003677 DNA binding*, and *GO:0008017*
335 *microtubule binding* (**Fig S30**). GO terms related to steroid metabolic processes (*GO:0008202*
336 *steroid metabolic process*) and oxidoreductase activity (*GO:0016705 oxidoreductase activity,*
337 *acting on paired donors, with incorporation or reduction of molecular oxygen*, *GO:0016712*
338 *oxidoreductase activity, acting on paired donors, with incorporation or reduction of molecular*
339 *oxygen, reduced flavin or flavoprotein as one donor, and incorporation of one atom of oxygen*)
340 were significantly enriched for the genes with significantly increased expression in the liver
341 samples for the response contrasts (**Fig 5**, **S29**). No GO terms were significantly enriched for

342 genes with significantly increased expression in the spleen samples for the response contrasts
343 (**Fig 5**).

344 GO terms related to blood coagulation (*GO:0007596 blood coagulation*) and the cell-
345 substrate junction (*GO:0030055 cell-substrate junction*) were significantly enriched for the
346 genes with significantly decreased expression in the blood samples for the response contrasts
347 (**Fig 5**, **S28**). GO terms related to receptor-mediated endocytosis were significantly enriched
348 for the genes with significantly decreased expression in the liver and lymph node samples for
349 the response contrasts (**Fig 5**). The top driver GO terms included *GO:0003823 antigen binding*
350 for the liver samples (**Fig S29**), and *GO:0071944 cell periphery*, *GO:0009986 cell surface*,
351 *GO:0007155 cell adhesion*, and *GO:0006897 endocytosis* for the lymph node samples (**Fig**
352 **S30**). GO terms related to multicellular development and morphogenesis including the driver
353 GO terms *GO:0007167 enzyme-linked receptor protein signaling pathway*, *GO:0032501*
354 *multicellular organismal process*, and *GO:0071495 cellular response to endogenous stimulus*
355 were also significantly enriched for the genes with significantly decreased expression in the
356 lymph node samples for the response contrasts (**Fig 5**, **S30**). GO terms related to cell migration
357 and motility (*GO:0016477 cell migration*, *GO:0048870 cell motility*) and cargo receptor
358 activity (*GO:0038024 cargo receptor activity*) were also enriched for these genes (**Fig 5**, **S30**).
359 GO terms related to the extracellular region (*GO:0005576 extracellular region*) were
360 significantly enriched for the genes with significantly decreased expression in both the lymph
361 node and spleen samples for the response contrasts (**Fig 5**, **S30**, **S31**), while GO terms related
362 to lipopolysaccharide binding (*GO:0001530 lipopolysaccharide binding*) were also
363 significantly enriched for the genes with significantly decreased expression in the spleen
364 samples for the response contrasts (**Fig 5**, **S31**).

365 For the direct contrasts, GO terms related to organelle metabolic processes were
366 significantly enriched for the genes with significantly increased expression in the blood, liver,
367 and lymph node samples (**Fig S32**). The GO term for leukocyte proliferation was significantly
368 enriched for genes with significantly increased expression in the blood samples, while GO
369 terms related to scavenger receptor activity and cell periphery were also significantly enriched
370 for genes with significantly increased expression in the lymph node samples (**Fig S32**). GO
371 terms related to receptor signalling pathways were significantly enriched for genes with
372 significantly decreased expression in the liver and lymph node samples, while GO terms related
373 to coagulation were significantly enriched for genes with significantly decreased expression in
374 the blood samples (**Fig S32**). GO terms related to actin binding and cytoskeleton, immune
375 response and antigen binding, small molecule and pyruvate metabolic processes, and the
376 cytosolic ribosome were also significantly enriched for genes with significantly decreased
377 expression in the liver samples (**Fig S32**). GO terms related to tube development, cell
378 migration, extracellular region, cell adhesion, and calcium ion binding were significantly
379 enriched for genes with significantly decreased expression in the lymph node samples (**Fig**
380 **S32**). GO terms related to metaphase chromosome alignment, the chromosome centromeric
381 region, and the microtubule cytoskeleton were significantly enriched for genes with
382 significantly decreased expression in the spleen samples (**Fig S32**).

383 For the N'Dama contrasts, GO terms related to cell process regulation were significantly
384 enriched for genes with significantly increased expression in all tissues (**Fig S33**). GO terms
385 related to GTPase activator activity, phagocytosis, and protein kinase binding were also
386 significantly enriched for genes with significantly increased expression in the liver samples
387 (**Fig S33**). GO terms related to cell development and regulation were significantly enriched for
388 genes with significantly decreased expression in all tissues (**Fig S33**). GO terms related to
389 metabolic processes, peroxisome organization, electron transfer activity, oxidoreductase

390 activity, and the endoplasmic reticulum membrane were enriched for genes with significantly
391 decreased expression in the liver samples (**Fig S33**). GO terms related to actin cytoskeleton
392 organization, extracellular matrix, cell projection, and vesicle-mediated transport were
393 significantly enriched for genes with significantly decreased expression in the lymph node and
394 spleen samples (**Fig S33**). GO terms related to the extracellular region were also significantly
395 enriched for genes with significantly decreased expression in the lymph node samples, while
396 GO terms related to extracellular matrix organization were significantly enriched for genes
397 with significantly decreased expression in the spleen samples (**Fig S33**). For the Boran
398 contrasts, GO terms related to cell process regulation were significantly enriched for genes with
399 significantly increased expression in all tissues and GO terms related to cell response regulation
400 were significantly enriched for genes with significantly decreased expression in all tissues,
401 while GO terms related to metabolic processes were also significantly enriched for genes with
402 significantly decreased expression in the liver and spleen samples (**Fig S34**).

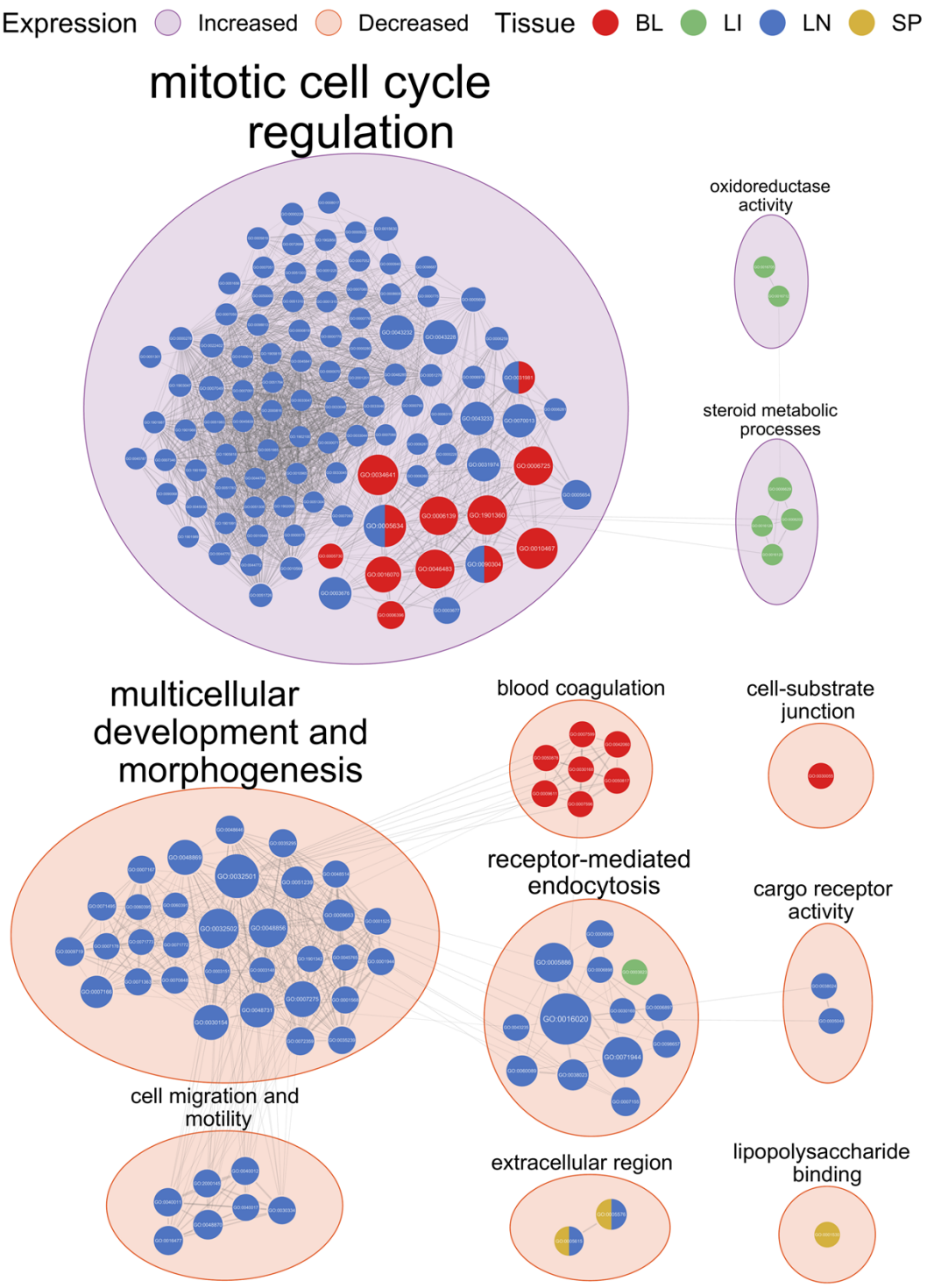

Fig 5. EnrichmentMap network of significantly enriched gene ontology (GO) terms identified from g:Profiler functional enrichment of significantly differentially expressed genes (DEGs) for the response contrasts. Each node represents a GO term with the colour of the node representing the tissue and the size representing the number of genes in the GO term. The edges indicate overlap between the GO terms with the width of the edges representing the similarity coefficient for the connected GO terms. The GO terms are clustered by AutoAnotate with the background colour of the clusters representing the direction of expression. The clusters are labelled with the size of the label scaling with the number of GO terms in the cluster.

413 # Discussion

414 The data filtering and normalisation steps resulted in a similar number of samples and
415 probe sets for analysis as previous studies that used Affymetrix® Bovine Genome Array data
416 sets to examine host responses to trypanosomiasis and other infectious diseases of cattle,
417 including the previous analysis of the liver, lymph node, and spleen samples [33, 91-93]. The
418 clear separation of the liver samples from the other tissues that is evident for PC1, which also
419 explained the majority of the total variation in the data set for PC1–10, may be due to several
420 factors (**Fig 2**). The first is biological differentiation between the liver samples and those of the
421 other tissues. This is supported by a previous gene expression microarray study using rat
422 (*Rattus norvegicus*) tissues, which also observed that PC1 in a PCA separated liver samples
423 from those taken from blood, lymph node, spleen, and other tissues [94]. This biological
424 difference may have been compounded by the higher number of liver samples in the data set
425 from Noyes and colleagues [33] due to the experimental design, which encompassed a larger
426 number of time points for the liver samples as well as a greater number of animals from which
427 the liver samples were taken to prevent the collection of multiple liver biopsies from the same
428 animal at consecutive time points [33]. This experimental design consideration also resulted in
429 more control liver samples for the pre-infection time point [33]. In total, 115 of the 211 samples
430 that passed the quality control filters or 54.50% of the filtered data set were liver samples
431 (**Table 1**). Because an unequal number of samples is known to increase the distance between
432 groups with larger sample sizes in a PCA, it is possible that the disproportionately large number
433 of liver samples in the present study has given rise to the effect seen in PC1 [95-97]. It is
434 therefore unsurprising that PC2, which explained a further 9.10% of the total variation in the
435 data set for PC1–10, separated the blood samples from the lymph node and spleen samples (**Fig**
436 **2**) as the blood samples were the second most numerous in the data set with 40 samples or
437 18.96% of the filtered data set (**Table 1**). It is not until PC5, which explained 1.32% of the total

438 variation in the data set for PC1–10, that the lymph node and spleen samples are separated (**Fig**
439 **S4**). The samples from these tissues are the least numerous in the data set with 29 spleen and
440 27 lymph node samples, making up 13.74% and 12.80% of the filtered data set, respectively
441 (**Table 1**). The spleen and lymph nodes are also both key components of the lymphatic and
442 immune systems and their functional and morphological similarities as hemopoietic organs that
443 filter bodily fluids have been long established [98-100]. It is logical, therefore, that these tissues
444 would show similar patterns of gene expression both before and after infection. The third and
445 fourth PCs (PC3 and PC4), which explained 2.24% and 1.78% of the total variation for PC1–
446 10, respectively, separated the samples temporally in order of dpi (**Fig S2**, **S3**). This illustrates
447 the overall similarity in response to infection across the populations and is in agreement with
448 RNA-seq data from whole blood samples taken during a similar trypanosome infection time
449 course experiment [42]. It also shows that the systemic response to trypanosome infection in
450 peripheral blood is distinct from that in the liver and other tissues and that blood sampling alone
451 may not be sufficient to capture all the tissue specific responses to infection.

452 Gene expression in bovine tissues can be measured using a variety of methods, one of
453 which is the Affymetrix® Bovine Genome Array based on GeneChip® technology [101] and
454 which contains more than 24,000 probe sets representing over 23,000 gene transcripts. The
455 Affymetrix® Bovine Genome Array platform has been previously used to study infectious
456 disease in cattle, including trypanosomiasis [33], and for mycobacterial infections that cause
457 tuberculosis and paratuberculosis [91-93]. Importantly, although expression microarrays have
458 been largely supplanted by RNA sequencing (RNA-seq), when the same biological samples
459 were analysed using both the Bovine Genome Array and RNA-seq, gene expression data
460 obtained using the two platforms were extremely well correlated in peripheral blood and
461 alveolar macrophages [102-104]. In addition, it has recently been shown that peripheral blood
462 gene expression data generated using RNA-seq, a different microarray technology (long

463 oligonucleotide microarrays), and reverse transcription quantitative real-time PCR (RT-qPCR)
464 were well correlated in independent studies of trypanosome infection in cattle [42].

465 The pattern of an increase in the numbers of significant DEGs until 21 days post infection
466 followed by a decrease before rising to a final peak at 35 days post infection across contrast
467 types and tissues (**Fig 3**, **S5–S8**) is consistent with known information about the cyclic nature
468 of parasitaemia during trypanosome infection, which has been shown to have an initial peak at
469 20 dpi [38]. It is also in agreement with the measures of parasitaemia in the blood samples
470 during this infection time course experiment, which showed peaks of parasitaemia from 15 to
471 22 dpi [41]. The final peak of significant DEGs at the end of the infection time course is
472 consistent with analysis of the same blood samples using a gene expression platform with less
473 gene content—a bovine long oligonucleotide (BLO) array—which detected the highest number
474 of significant DEGs between the two populations at 34 dpi [40]. It is also in agreement with a
475 study using RNA-seq data from whole blood samples that found the highest number of DEGs
476 in N'Dama samples at the end of a similar trypanosome infection time course experiment [42].
477 The higher numbers of significant DEGs in the N'Dama contrasts when compared to the Boran
478 contrasts is in agreement with previous results and supports the hypothesis that, compared to
479 trypanosusceptible Boran, trypanotolerant N'Dama cattle exhibit an earlier proinflammatory
480 response, which is evident in both PBMC and whole peripheral blood [40-42]. That the
481 response contrasts had the lowest number of significant DEGs is to be expected given that these
482 contrasts are examining the data set for differences in the rate of change of gene expression
483 between the populations [33]. In addition, the numbers of significant DEGs for the response
484 contrasts were similar to those found in the original analysis by Noyes and colleagues [33],
485 which employed a similar approach. The numbers of genes in common between the contrasts
486 is to be expected due to the shared underlying data set while the numbers of genes in common
487 within the contrasts is likely due to similar patterns of gene expression found across the

488 populations, tissues, and time points during the infection (**Fig S9–S13**). This is in agreement
489 with RNA-seq data that showed large overlaps in DEGs in response to trypanosome infection
490 between five different cattle populations with varying levels of trypanotolerance [42].

491 The similarities in gene expression are also illustrated by the high level of overlap in the
492 top 10 most significant DEGs with increased and decreased expression between the contrasts
493 (**Table 2**, **S3–S5**). The most common genes in the top 10 most significant DEGs for all the
494 contrasts included those related to the immune system, such as the most common significant
495 DEG—the thymosin beta 10 gene (*TMSB10*), which has been identified as a hub gene in the
496 response to Rift Valley fever (RVF), an important viral disease in African cattle [105]. Other
497 immune-related genes in the set of the most common genes in the top 10 most significant DEGs
498 for all the contrasts included the CYFIP related Rac1 interactor B gene (*CYRIB*), which encodes
499 a regulator of phagocytosis [106], and the protein tyrosine phosphatase receptor type C gene
500 (*PTPRC*), which is an essential regulator of T and B cell antigen receptor-mediated activation
501 and has been highlighted by multiple studies of trypanosome infection in mice [107-112].
502 Similarly, the Spi-1 proto-oncogene gene (*SPI1*), which encodes a transcription factor that
503 activates gene expression during myeloid and B-lymphoid cell development, has also been
504 implicated as an important host gene in trypanosome infection in the mouse [111, 113]. The
505 presence of immune genes in the top 10 most significant DEGs is to be expected given the
506 nature of the infection time course experiment and is in agreement with previous results from
507 this and other infection experiments, illustrating the similarity in immune responses between
508 the N'Dama and Boran cattle during trypanosome infection [33, 40, 42].

509 The most common genes in the top 10 most significant DEGs for the response contrasts
510 included genes which are involved in in inflammation and immunity such as the olfactomedin
511 4 gene (*OLFM4*) and the transmembrane protein 45B gene (*TMEM45B*) [114, 115]. Other

512 common genes in the top 10 most significant DEGs for the response contrasts are more varied
513 in function and included the cytochrome P450 family 4 subfamily B member 1 gene (*CYP4B1*),
514 which is involved in drug metabolism [116]; the RAB31, member RAS oncogene family gene
515 (*RAB31*), which is a small GTPase [117]; and the TTL family tubulin polyglutamylase complex
516 subunit L1 gene (*TTLL1*), which is involved in microtubule cytoskeleton organisation [118].

517 The top 10 most significant DEGs for the response contrasts also included genes
518 encoding antimicrobial peptides (AMPs), which are key components of the innate immune
519 system that have huge therapeutic potential and are important for the healthy function of a
520 variety of bovine tissues [119-122]. This is in agreement with previous RT-qPCR results using
521 blood samples from the same time course infection experiment; in this regard, it has previously
522 been hypothesised that trypanotolerance may be partly due to inherited regulatory sequence
523 variation in genes encoding antimicrobial peptides [39]. For example, the liver enriched
524 antimicrobial peptide 2 gene (*LEAP2*) [123], which was in the top 10 most significant DEGs
525 with decreased expression for the liver samples at 21 and 35 dpi for the response contrasts
526 (**Table 2**). The previous RT-qPCR results showed that *LEAP2* exhibited significantly
527 decreased expression in N'Dama samples at 34 dpi relative to day 0 while the Boran animals
528 showed no such change [39]. Other AMP genes in the top 10 most significant DEGs for the
529 response contrasts which examine the N'Dama samples relative to the Boran samples included
530 the cathelicidin antimicrobial peptide gene (*CATHL3*) [124] with decreased expression in the
531 spleen samples at 35 dpi, which is notable since cathelicidins were found to be the most
532 effective of the three classes of AMP at killing both insect and bloodstream forms of *T. brucei*
533 in mice [125]; the defensin beta 4A gene (*DEFB4A*) [126] with increased expression in the
534 lymph node samples at 35 dpi; and S100 calcium binding protein A7 gene (*S100A7*) [127] with
535 increased expressed in peripheral blood at 25 dpi (**Table 2**) [39, 124, 126, 127].

536 Another group of genes represented in the top 10 most significant DEGs for the response
537 contrasts were cytokine genes (**Table 2**). This is consistent with both RT-qPCR and BLO
538 microarray results from the same infection time course experiment and previous studies using
539 the same animals [33, 40, 41]. This observation agrees with more recent transcriptomics studies
540 from trypanotolerant and trypanosusceptible cattle and studies of trypanosome infection in the
541 mouse [42, 128]. These genes included the C-C motif chemokine ligand 20 gene (*CCL20*) with
542 increased expression in the lymph node samples at 35 dpi; the C-X-C motif chemokine ligand
543 11 (*CXCL11*) with increased expression in the liver samples at 12 dpi; the C-X-C motif
544 chemokine ligand 13 gene (*CXCL13*) with increased expression in the lymph node samples at
545 21 dpi; the C-X-C motif chemokine ligand 16 gene (*CXCL16*) with decreased expression in the
546 spleen samples 35 dpi; the C-X-C motif chemokine ligand 17 gene (*CXCL17*) with decreased
547 expression in the liver samples at 15 dpi; the interleukin 33 gene (*IL33*) with decreased
548 expression in the lymph node samples at 35 dpi; and the TNF superfamily member 13b gene
549 (*TNFSF13B*) with increased expression in the lymph node samples at 21 dpi (**Table 2**).

550 Related genes such as cytokine receptors and inhibitors were also in the top 10 most
551 significant DEGs for the response contrasts (**Table 2**). These included the C-C motif
552 chemokine receptor 7 gene (*CCR7*) with decreased expression in the blood samples at 25 and
553 34 dpi; the C1q and TNF related 5 gene (*C1QTNF5*) with decreased expression in lymph node
554 samples at 35 dpi; and the interleukin 18 binding protein gene (*IL18BP*) with increased
555 expression in the liver samples at 12 dpi (**Table 2**). Additionally, mitogen-activated protein
556 kinase (MAPK) genes were present in the top 10 most significant DEGs, which is in agreement
557 with previous work using the same animals and also a more recent study of trypanosome
558 infection in cattle [33, 40, 42]. In this regard, it is notable that MAPK signalling pathways are
559 involved in the response to proinflammatory cytokines and are known to be subverted by *T.*
560 *cruzi* and other trypanosomatid parasites to evade the host immune response [129-131].

561 A final notable group of genes present in the top 10 most significant DEGs were those
562 encoding apolipoproteins, including apolipoprotein B (*APOB*) with decreased expression for
563 the response contrast in the liver samples at 12 dpi (**Table 2**); apolipoprotein L3 (*APOL3*) with
564 increased expression for the direct contrast in the blood samples at 25 dpi (**Table S3**); and
565 apolipoprotein M (*APOM*) with decreased expression for the Boran contrast in the liver
566 samples at 15 dpi (**Table S5**). These genes are related to apolipoprotein 1 (*APOL1*) which
567 encodes the protein that makes up the trypanosome lytic factor (TLF) that is present in human
568 and western lowland gorilla (*Gorilla gorilla gorilla*) serum [132]. TLF is taken up by
569 susceptible trypanosomes where it interferes with their lysosomes and mitochondria, thereby
570 conferring host resistance to most trypanosome species [132]. It is therefore interesting that
571 related genes are among the top 10 most differentially expressed in this study.

572 Gene ontology terms related to regulation of the mitotic cell cycle, steroid metabolic
573 processes and oxidoreductase activity (**Fig 5**) were significantly enriched for the genes with
574 significantly increased expression for the response contrasts, which is in agreement with results
575 from a previous study using the same animals [33]. The overlap and grouping of the GO terms
576 between the blood and lymph node samples illustrates the similarity of responses to infection
577 for these tissues. The lack of GO terms significantly enriched for genes with significantly
578 increased expression for the response contrasts in the spleen samples (**Fig 5**) can be explained
579 by the lower numbers of significant DEGs with increased expression for these samples (**Fig 3**,
580 **S5**). A larger range of GO terms were significantly enriched for the genes with significantly
581 decreased expression for the response contrasts (**Fig 5**). This is likely due to the higher number
582 of significant DEGs with decreased expression, which would allow more GO terms to be
583 significantly enriched for these genes (**Fig 3**). The GO terms significantly enriched for the
584 genes with significantly decreased expression for the response contrasts included those related
585 to multicellular development and morphogenesis, receptor-mediated endocytosis, cell

586 migration and motility, cargo receptor activity, extracellular region, and lipopolysaccharide
587 binding (**Fig 5**). These observations are also in agreement with results of the previous analysis
588 using the same animals [33].

589 It is logical that the GO terms that are significantly enriched for genes with significantly
590 decreased expression for the response contrasts are related to blood coagulation in the PBMC
591 samples (**Fig 5**, **S28**). The effects of blood-borne trypanosome parasites on the blood of the
592 host have been long studied in both cattle and humans [133-135]. Notably, anaemia is the main
593 cause of death due trypanosomiasis and the ability to control this anaemia is consider critical
594 to trypanotolerance in cattle [136, 137]. While trypanosomes do obtain iron from their
595 environment in the blood of the host and that iron homeostasis and metabolism in the
596 trypanosome parasite are known to be essential for infection, it has been observed that anaemia
597 does not correlate with parasitaemia [138-141]. Additionally, trypanosomes require much less
598 iron than a mammalian cell [142, 143]. The anaemia caused by trypanosome infection is
599 therefore considered to be an immune response, which may be driven by cytokines [137, 144,
600 145].

601 During trypanosome infection in cattle, control of anaemia and parasitaemia are key
602 components of trypanotolerance but are considered to represent separate genetically
603 determined traits [146]. This is exemplified by genes related to iron ion homeostasis such as
604 the solute carrier family 40 member 1 gene (*SLC40A1*) [147], which was noted to be among
605 the most divergent between trypanotolerant N'Dama and trypanosusceptible Boran as a result
606 of a marked reduction in expression in the N'Dama population over the course of the infection
607 experiment relative to the pre-infection level in PBMC [40]. *SLC40A1* was also in the top 10
608 most significant DEGs with decreased expression in the blood samples at 34 dpi for the
609 response contrast in this study, highlighting the divergent nature of the expression of this gene

610 between the N'Dama and Boran populations during trypanosome infection (**Table 2**). The
611 reduction of cellular iron export by the SLC40A1 protein is thought to be a component of an
612 innate immune-driven strategy to prevent bloodstream pathogens from accessing iron, with
613 anaemia as a side effect for the host [137, 140, 144]. A related gene, the solute carrier family
614 11 member 1 gene (*SLC11A1*), which regulates iron homeostasis in macrophages was found to
615 be differentially expressed between N'Dama and African indicine cattle during trypanosome
616 infection using RNA-seq data [42] and variants of this gene are associated with susceptibility
617 to several infectious diseases, including tuberculosis in cattle [148, 149]. Finally, it is
618 noteworthy that the previous work by Noyes and colleagues [33], which used a different
619 functional enrichment approach also highlighted biological pathways related to iron ion
620 homeostasis.

621 The significantly enriched GO terms showed similar patterns for the direct contrasts with
622 those enriched for the genes with significantly increased expression related to organelle
623 metabolic processes for multiple tissues, while those enriched for the genes with significantly
624 decreased expression showed a greater range of processes (**Fig S32**). Gene ontology terms
625 related to coagulation were also significantly enriched for genes with significantly decreased
626 expression in the PBMC samples (**Fig S32**). For the N'Dama and Boran contrasts, the
627 significantly enriched GO terms were related to cell regulation across all tissues, time points,
628 and direction of expression (**Fig S33**, **S34**). This is likely a result of the higher numbers of
629 significant DEGs for these contrasts, which led to higher numbers of significantly enriched GO
630 terms that were too varied for the EnrichmentMap method to summarise effectively (**Fig 3**)
631 [84].

632 In conclusion, trypanotolerant N'Dama and trypanosusceptible Boran cattle responded
633 in largely similar ways during trypanosome infection when gene expression was examined

634 using PBMC, liver, lymph node, and spleen samples with peaks and troughs of gene expression
635 following the cyclic pattern of parasitaemia exhibited during trypanosome infection.
636 Differences in response to infection between the two populations include genes related to the
637 immune system such as those encoding antimicrobial peptides and cytokines. Within the
638 PBMC samples, differences in genes relating to coagulation and iron homeostasis support the
639 hypothesis that the dual abilities to control both parasitaemia and the anaemia resulting from
640 the innate immune response to trypanosome parasites are key to trypanotolerance. This work
641 adds to our understanding of host-trypanosome interactions across multiple tissues and time
642 points as well as to our knowledge of how genetic variation underlying the host response can
643 lead to differential host tolerance of, or susceptibility to, trypanosome infection. This improves
644 our general understanding of mammalian trypanosome infection which may also be applicable
645 to human African trypanosomiasis.

Acknowledgements

We thank Morris Agaba, Olivier Hanotte, Stephen J. Kemp, and Stephen V. Gordon for assistance with sample resources and for useful scientific discussion.

649 # References

650 1. Steverding D. The history of African trypanosomiasis. Parasit Vectors. 2008;1(1):3.
651 Epub 20080212. https://doi.org/10.1186/1756-3305-1-3. PubMed PMID: 18275594.

652 2. Brun R, Blum J, Chappuis F, Burri C. Human African trypanosomiasis. Lancet.
653 2010;375(9709):148-59. Epub 20091014. https://doi.org/10.1016/S0140-6736(09)60829-1.
654 PubMed PMID: 19833383.

655 3. Taylor KA. Immune responses of cattle to African trypanosomes: protective or
656 pathogenic? Int J Parasitol. 1998;28(2):219-40. https://doi.org/10.1016/s0020-7519(97)00154-
657 9. PubMed PMID: 9512986.

658 4. Taylor KA, Mertens B. Immune response of cattle infected with African trypanosomes.
659 Mem Inst Oswaldo Cruz. 1999;94(2):239-44. https://doi.org/10.1590/s0074-
660 02761999000200022. PubMed PMID: 10224536.

661 5. Ibrahim MAM, Weber JS, Ngomtcho SCH, Signaboubo D, Berger P, Hassane HM, et
662 al. Diversity of trypanosomes in humans and cattle in the HAT foci Mandoul and Maro,
663 Southern Chad-A matter of concern for zoonotic potential? PLoS Negl Trop Dis.
664 2021;15(6):e0009323. Epub 20210609. https://doi.org/10.1371/journal.pntd.0009323.
665 PubMed PMID: 34106914.

666 6. Hounyèmè RE, Kaboré J, Gimonneau G, Somda MB, Salou E, Missihoun AA, et al.
667 Molecular epidemiology of Animal African Trypanosomosis in southwest Burkina Faso. PLoS
668 Negl Trop Dis. 2022;16(8):e0010106. Epub 20220822.
669 https://doi.org/10.1371/journal.pntd.0010106. PubMed PMID: 35994491.

670 7. N'Djetchi MK, Ilboudo H, Koffi M, Kaboré J, Kaboré JW, Kaba D, et al. The study of
671 trypanosome species circulating in domestic animals in two human African trypanosomiasis
672 foci of Côte d'Ivoire identifies pigs and cattle as potential reservoirs of Trypanosoma brucei
673 gambiense. PLoS Negl Trop Dis. 2017;11(10):e0005993. Epub 20171018.
674 https://doi.org/10.1371/journal.pntd.0005993. PubMed PMID: 29045405.

675 8. Antoine-Moussiaux N, Magez S, Desmecht D. Contributions of experimental mouse
676 models to the understanding of African trypanosomiasis. Trends Parasitol. 2008;24(9):411-8.
677 Epub 20080804. https://doi.org/10.1016/j.pt.2008.05.010. PubMed PMID: 18684669.

678 9. Magez S, Caljon G. Mouse models for pathogenic African trypanosomes: unravelling
679 the immunology of host-parasite-vector interactions. Parasite Immunol. 2011;33(8):423-9.
680 https://doi.org/10.1111/j.1365-3024.2011.01293.x. PubMed PMID: 21480934.

681 10. Moulton JE, Stevens DR. Animal model of human disease: trypanosomiasis, sleeping
682 sickness. Am J Pathol. 1978;91(3):693-6. PubMed PMID: 655266.

683 11. Kao WH, Klag MJ, Meoni LA, Reich D, Berthier-Schaad Y, Li M, et al. *MYH9* is
684 associated with nondiabetic end-stage renal disease in African Americans. Nat Genet.
685 2008;40(10):1185-92. Epub 2008/09/17. https://doi.org/10.1038/ng.232. PubMed PMID:
686 18794854.

687 12. Genovese G, Friedman DJ, Ross MD, Lecordier L, Uzureau P, Freedman BI, et al.
688 Association of trypanolytic ApoL1 variants with kidney disease in African Americans. Science.
689 2010;329(5993):841-5. Epub 2010/07/22. https://doi.org/10.1126/science.1193032. PubMed
690 PMID: 20647424.

691 13. Berthier D, Breniere SF, Bras-Goncalves R, Lemesre JL, Jamonneau V, Solano P, et
692 al. Tolerance to trypanosomatids: a threat, or a key for disease elimination? Trends Parasitol.
693 2016;32(2):157-68. Epub 20151128. https://doi.org/10.1016/j.pt.2015.11.001. PubMed PMID:
694 26643519.

695 14. Kemp SJ, Teale AJ. Genetic basis of trypanotolerance in cattle and mice. Parasitol
696 Today. 1998;14(11):450-4. https://doi.org/10.1016/s0169-4758(98)01334-9. PubMed PMID:
697 17040846.

698 15. Truc P, Büscher P, Cuny G, Gonzatti MI, Jannin J, Joshi P, et al. Atypical human
699 infections by animal trypanosomes. PLoS Negl Trop Dis. 2013;7(9):e2256. Epub 20130912.
700 https://doi.org/10.1371/journal.pntd.0002256. PubMed PMID: 24069464.

701 16. Kumar R, Gupta S, Bhutia WD, Vaid RK, Kumar S. Atypical human trypanosomosis:
702 Potentially emerging disease with lack of understanding. Zoonoses Public Health.
703 2022;69(4):259-76. Epub 20220330. https://doi.org/10.1111/zph.12945. PubMed PMID:
704 35355422.

705 17. Okello I, Mafie E, Eastwood G, Nzalawahe J, Mboera LEG. African animal
706 trypanosomiasis: a systematic review on prevalence, risk factors and drug resistance in sub-

707 Saharan Africa. J Med Entomol. 2022;59(4):1099-143. https://doi.org/10.1093/jme/tjac018.
708 PubMed PMID: 35579072.

709 18. Herrero M, Thornton PK. Livestock and global change: emerging issues for sustainable
710 food systems. Proc Natl Acad Sci U S A. 2013;110(52):20878-81. Epub 2013/12/18.
711 https://doi.org/10.1073/pnas.1321844111. PubMed PMID: 24344313.

712 19. Thornton PK. Livestock production: recent trends, future prospects. Philos Trans R Soc
713 Lond B Biol Sci. 2010;365(1554):2853-67. Epub 2010/08/18.
714 https://doi.org/10.1098/rstb.2010.0134. PubMed PMID: 20713389.

715 20. Hanotte O, Bradley DG, Ochieng JW, Verjee Y, Hill EW, Rege JE. African
716 pastoralism: genetic imprints of origins and migrations. Science. 2002;296(5566):336-9.
717 PubMed PMID: 11951043.

718 21. MacHugh DE, Shriver MD, Loftus RT, Cunningham P, Bradley DG. Microsatellite
719 DNA variation and the evolution, domestication and phylogeography of taurine and zebu cattle
720 (Bos taurus and Bos indicus). Genetics. 1997;146(3):1071-86. Epub 1997/07/01.
721 https://doi.org/10.1093/genetics/146.3.1071. PubMed PMID: 9215909.

722 22. Kim J, Hanotte O, Mwai OA, Dessie T, Bashir S, Diallo B, et al. The genome landscape
723 of indigenous African cattle. Genome Biol. 2017;18(1):34. Epub 20170220.
724 https://doi.org/10.1186/s13059-017-1153-y. PubMed PMID: 28219390.

725 23. Mwai O, Hanotte O, Kwon YJ, Cho S. African indigenous cattle: unique genetic
726 resources in a rapidly changing world. Asian-Australas J Anim Sci. 2015;28(7):911-21. Epub
727 2015/06/25. https://doi.org/10.5713/ajas.15.0002R. PubMed PMID: 26104394.

728 24. Holden CJ. Bantu language trees reflect the spread of farming across sub-Saharan
729 Africa: a maximum-parsimony analysis. Proc Biol Sci. 2002;269(1493):793-9.
730 https://doi.org/10.1098/rspb.2002.1955. PubMed PMID: 11958710.

731 25. Tishkoff SA, Reed FA, Friedlaender FR, Ehret C, Ranciaro A, Froment A, et al. The
732 genetic structure and history of Africans and African Americans. Science.
733 2009;324(5930):1035-44. Epub 20090430. https://doi.org/10.1126/science.1172257. PubMed
734 PMID: 19407144.

735 26. Yaro M, Munyard KA, Stear MJ, Groth DM. Combatting African animal
736 trypanosomiasis (AAT) in livestock: the potential role of trypanotolerance. Vet Parasitol.
737 2016;225:43-52. Epub 20160504. https://doi.org/10.1016/j.vetpar.2016.05.003. PubMed
738 PMID: 27369574.

739 27. Freeman AR, Meghen CM, MacHugh DE, Loftus RT, Achukwi MD, Bado A, et al.
740 Admixture and diversity in West African cattle populations. Mol Ecol. 2004;13(11):3477-87.
741 https://doi.org/10.1111/j.1365-294X.2004.02311.x. PubMed PMID: 15488005.

742 28. Murray M, Trail JC, D'Ieteren GD. Trypanotolerance in cattle and prospects for the
743 control of trypanosomiasis by selective breeding. Rev Sci Tech. 1990;9(2):369-86.
744 https://doi.org/10.20506/rst.9.2.506. PubMed PMID: 2132686.

745 29. Murray M, Black SJ. African trypanosomiasis in cattle: working with nature's solution.
746 Vet Parasitol. 1985;18(2):167-82. https://doi.org/10.1016/0304-4017(85)90065-2. PubMed
747 PMID: 3898544.

748 30. d'Ieteren GD, Authié E, Wissocq N, Murray M. Trypanotolerance, an option for
749 sustainable livestock production in areas at risk from trypanosomosis. Rev Sci Tech.
750 1998;17(1):154-75. https://doi.org/10.20506/rst.17.1.1088. PubMed PMID: 9638808.

751 31. Trail JC, D'Ieteren GD, Teale AJ. Trypanotolerance and the value of conserving
752 livestock genetic resources. Genome. 1989;31(2):805-12. https://doi.org/10.1139/g89-142.
753 PubMed PMID: 2534387.

754 32. Smetko A, Soudre A, Silbermayr K, Muller S, Brem G, Hanotte O, et al.
755 Trypanosomosis: potential driver of selection in African cattle. Front Genet. 2015;6:137. Epub
756 20150421. https://doi.org/10.3389/fgene.2015.00137. PubMed PMID: 25964796.

757 33. Noyes H, Brass A, Obara I, Anderson S, Archibald AL, Bradley DG, et al. Genetic and
758 expression analysis of cattle identifies candidate genes in pathways responding to
759 *Trypanosoma congolense* infection. Proc Natl Acad Sci U S A. 2011;108(22):9304-9. Epub
760 20110518. https://doi.org/10.1073/pnas.1013486108. PubMed PMID: 21593421.

761 34. Naessens J, Teale AJ, Sileghem M. Identification of mechanisms of natural resistance
762 to African trypanosomiasis in cattle. Vet Immunol Immunopathol. 2002;87(3-4):187-94.
763 https://doi.org/10.1016/s0165-2427(02)00070-3. PubMed PMID: 12072233.

764 35. Trail JC, d'Ieteren GD, Maille JC, Yangari G. Genetic aspects of control of anaemia
765 development in trypanotolerant N'Dama cattle. Acta Trop. 1991;48(4):285-91.
766 https://doi.org/10.1016/0001-706x(91)90016-d. PubMed PMID: 1674402.

767 36. Gautier M, Flori L, Riebler A, Jaffrezic F, Laloe D, Gut I, et al. A whole genome
768 Bayesian scan for adaptive genetic divergence in West African cattle. BMC Genomics.
769 2009;10:550. Epub 20091121. https://doi.org/10.1186/1471-2164-10-550. PubMed PMID:
770 19930592.

771 37. Kim SJ, Ka S, Ha JW, Kim J, Yoo D, Kim K, et al. Cattle genome-wide analysis reveals
772 genetic signatures in trypanotolerant N'Dama. BMC Genomics. 2017;18(1):371. Epub
773 20170512. https://doi.org/10.1186/s12864-017-3742-2. PubMed PMID: 28499406.

774 38. Hill EW, O'Gorman GM, Agaba M, Gibson JP, Hanotte O, Kemp SJ, et al.
775 Understanding bovine trypanosomiasis and trypanotolerance: the promise of functional
776 genomics. Vet Immunol Immunopathol. 2005;105(3-4):247-58.
777 https://doi.org/10.1016/j.vetimm.2005.02.004. PubMed PMID: 15808304.

778 39. Meade KG, O'Gorman GM, Hill EW, Narciandi F, Agaba M, Kemp SJ, et al. Divergent
779 antimicrobial peptide (AMP) and acute phase protein (APP) responses to *Trypanosoma*
780 *congolense* infection in trypanotolerant and trypanosusceptible cattle. Mol Immunol.
781 2009;47(2-3):196-204. Epub 20091103. https://doi.org/10.1016/j.molimm.2009.09.042.
782 PubMed PMID: 19889461.

783 40. O'Gorman GM, Park SD, Hill EW, Meade KG, Coussens PM, Agaba M, et al.
784 Transcriptional profiling of cattle infected with *Trypanosoma congolense* highlights gene
785 expression signatures underlying trypanotolerance and trypanosusceptibility. BMC Genomics.
786 2009;10:207. Epub 20090501. https://doi.org/10.1186/1471-2164-10-207. PubMed PMID:
787 19409086.

788 41. O'Gorman GM, Park SD, Hill EW, Meade KG, Mitchell LC, Agaba M, et al. Cytokine
789 mRNA profiling of peripheral blood mononuclear cells from trypanotolerant and
790 trypanosusceptible cattle infected with *Trypanosoma congolense*. Physiol Genomics.
791 2006;28(1):53-61. Epub 20060919. https://doi.org/10.1152/physiolgenomics.00100.2006.
792 PubMed PMID: 16985010.

42. Peylhard M, Berthier D, Dayo G-K, Chantal I, Sylla S, Nidelet S, et al. Whole blood transcriptome profiles of trypanotolerant and trypanosusceptible cattle highlight a differential modulation of metabolism and immune response during infection by *Trypanosoma congolense*. Peer Community J. 2023;3. https://doi.org/10.24072/pcjournal.239.

43. Dayo GK, Gautier M, Berthier D, Poivey JP, Sidibe I, Bengaly Z, et al. Association studies in QTL regions linked to bovine trypanotolerance in a West African crossbred population. Anim Genet. 2012;43(2):123-32. Epub 20110722. https://doi.org/10.1111/j.1365-2052.2011.02227.x. PubMed PMID: 22404348.

44. Bahbahani H, Afana A, Wragg D. Genomic signatures of adaptive introgression and environmental adaptation in the Sheko cattle of southwest Ethiopia. PLoS ONE. 2018;13(8):e0202479. Epub 20180816. https://doi.org/10.1371/journal.pone.0202479. PubMed PMID: 30114214.

45. Berthier D, Peylhard M, Dayo GK, Flori L, Sylla S, Bolly S, et al. A comparison of phenotypic traits related to trypanotolerance in five west african cattle breeds highlights the value of shorthorn taurine breeds. PLoS ONE. 2015;10(5):e0126498. Epub 2015/05/09. https://doi.org/10.1371/journal.pone.0126498. PubMed PMID: 25954819.

46. Alvarez I, Perez-Pardal L, Traore A, Fernandez I, Goyache F. Lack of haplotype structuring for two candidate genes for trypanotolerance in cattle. J Anim Breed Genet. 2016;133(2):105-14. Epub 20150914. https://doi.org/10.1111/jbg.12181. PubMed PMID: 26365013.

47. Goyache F, Perez-Pardal L, Fernandez I, Traore A, Menendez-Arias NA, Alvarez I. Ancient autozygous segments subject to positive selection suggest adaptive immune responses in West African cattle. Gene. 2021;803:145899. Epub 20210813. https://doi.org/10.1016/j.gene.2021.145899. PubMed PMID: 34400278.

48. Rajavel A, Heinrich F, Schmitt AO, Gultas M. Identifying cattle breed-specific partner choice of transcription factors during the African trypanosomiasis disease progression using bioinformatics analysis. Vaccines (Basel). 2020;8(2). Epub 20200523. https://doi.org/10.3390/vaccines8020246. PubMed PMID: 32456126.

821 49. Rajavel A, Klees S, Hui Y, Schmitt AO, Gultas M. Deciphering the molecular
822 mechanism underlying African animal trypanosomiasis by means of the 1000 Bull Genomes
823 Project genomic dataset. Biology (Basel). 2022;11(5). Epub 20220513.
824 https://doi.org/10.3390/biology11050742. PubMed PMID: 35625470.

825 50. Geigy R, Kauffmann M. Sleeping sickness survey in the Serengeti area (Tanzania)
826 1971. I. Examination of large mammals for trypanosomes. Acta Trop. 1973;30(1):12-23.
827 PubMed PMID: 4144952.

828 51. Nantulya VM, Musoke AJ, Rurangirwa FR, Moloo SK. Resistance of cattle to tsetse-
829 transmitted challenge with *Trypanosoma brucei* or *Trypanosoma congolense* after spontaneous
830 recovery from syringe-passaged infections. Infect Immun. 1984;43(2):735-8.
831 https://doi.org/10.1128/iai.43.2.735-738.1984. PubMed PMID: 6693173.

832 52. Akol GW, Murray M. Early events following challenge of cattle with tsetse infected
833 with *Trypanosoma congolense*: development of the local skin reaction. Vet Rec.
834 1982;110(13):295-302. https://doi.org/10.1136/vr.110.13.295. PubMed PMID: 7072104.

835 53. Dwinger RH, Murray M, Moloo SK. Potential value of localized skin reactions
836 (chancres) induced by *Trypanosoma congolense* transmitted by *Glossina morsitans centralis*
837 for the analysis of metacyclic trypanosome populations. Parasite Immunol. 1987;9(3):353-62.
838 https://doi.org/10.1111/j.1365-3024.1987.tb00513.x. PubMed PMID: 3601446.

839 54. Frerebeau N. khroma: Colour Schemes for Scientific Data Visualization. manual. 2023
840 2023. Report No.

841 55. Garnier, Simon, Ross, Noam, Rudis, Robert, et al. viridis(Lite) - Colorblind-Friendly
842 Color Maps for R. manual. 2023 2023. Report No.

843 56. Gautier L, Cope L, Bolstad BM, Irizarry RA. *affy*—analysis of Affymetrix GeneChip
844 data at the probe level. Bioinformatics. 2004;20(3):307-15.
845 https://doi.org/10.1093/bioinformatics/btg405. PubMed PMID: 14960456.

846 57. Huber W, Carey VJ, Gentleman R, Anders S, Carlson M, Carvalho BS, et al.
847 Orchestrating high-throughput genomic analysis with Bioconductor. Nat Methods.
848 2015;12(2):115-21. https://doi.org/10.1038/nmeth.3252. PubMed PMID: 25633503.

849 58. Kauffmann A, Gentleman R, Huber W. arrayQualityMetrics—a bioconductor package
850 for quality assessment of microarray data. Bioinformatics. 2009;25(3):415-6. Epub 20081223.
851 https://doi.org/10.1093/bioinformatics/btn647. PubMed PMID: 19106121.

852 59. R Core Team. R: A Language and Environment for Statistical Computing. manual.
853 Vienna, Austria: R Foundation for Statistical Computing, 2023 2023. Report No.

854 60. Rue-Albrecht K, Magee DA, Killick KE, Nalpas NC, Gordon SV, MacHugh DE.
855 Comparative functional genomics and the bovine macrophage response to strains of the
856 *Mycobacterium* genus. Front Immunol. 2014;5:536. Epub 20141105.
857 https://doi.org/10.3389/fimmu.2014.00536. PubMed PMID: 25414700.

858 61. Hochreiter S, Clevert DA, Obermayer K. A new summarization method for Affymetrix
859 probe level data. Bioinformatics. 2006;22(8):943-9. Epub 20060210.
860 https://doi.org/10.1093/bioinformatics/btl033. PubMed PMID: 16473874.

861 62. Wickham H, François R, Henry L, Müller K, Vaughan D. dplyr: A Grammar of Data
862 Manipulation. manual. 2023 2023. Report No.

863 63. van den Brand T. ggh4x: Hacks for 'ggplot2'. manual. 2023 2023. Report No.

864 64. Wickham H. ggplot2: Elegant Graphics for Data Analysis. New York: Springer; 2009.

865 65. Wilke CO, Wiernik BM. ggtext: Improved Text Rendering Support for 'ggplot2'.
866 manual. 2022.

867 66. Bache SM, Wickham H. magrittr: A Forward-Pipe Operator for R. manual. 2022 2022.
868 Report No.

869 67. Wickham H, Hester J, Bryan J. readr: Read Rectangular Text Data. manual. 2023 2023.
870 Report No.

871 68. Wickham H. Reshaping data with the reshape package. J Stat Softw. 2007;21(12):1 -
872 20. https://doi.org/10.18637/jss.v021.i12.

873 69. Wickham H. stringr: Simple, Consistent Wrappers for Common String Operations.
874 manual. 2023 2023. Report No.

875 70. Ritchie ME, Phipson B, Wu D, Hu Y, Law CW, Shi W, et al. limma powers differential
876 expression analyses for RNA-sequencing and microarray studies. Nucleic Acids Res.
877 2015;43(7):e47. Epub 20150120. https://doi.org/10.1093/nar/gkv007. PubMed PMID:
878 25605792.

879 71. Pedersen TL. patchwork: The Composer of Plots. manual. 2023 2023. Report No.

880 72. Smyth GK, Michaud J, Scott HS. Use of within-array replicate spots for assessing
881 differential expression in microarray experiments. Bioinformatics. 2005;21(9):2067-75. Epub
882 20050118. https://doi.org/10.1093/bioinformatics/bti270. PubMed PMID: 15657102.

883 73. Smyth GK. Linear models and empirical bayes methods for assessing differential
884 expression in microarray experiments. Stat Appl Genet Mol Biol. 2004;3:Article3. Epub
885 20040212. https://doi.org/10.2202/1544-6115.1027. PubMed PMID: 16646809.

886 74. Benjamini Y, Hochberg Y. Controlling the false discovery rate: a practical and
887 powerful approach to multiple testing. J Roy Stat Soc B Met. 1995;57(1):289-300.

888 75. Kolberg L, Raudvere U, Kuzmin I, Adler P, Vilo J, Peterson H. g:Profiler-interoperable
889 web service for functional enrichment analysis and gene identifier mapping (2023 update).
890 Nucleic Acids Res. 2023;51(W1):W207-W12. https://doi.org/10.1093/nar/gkad347. PubMed
891 PMID: 37144459.

892 76. Krassowski M. ComplexUpset. manual. 2020 2020. Report No.

893 77. Slowikowski K. ggrepel: Automatically Position Non-Overlapping Text Labels with
894 'ggplot2'. manual. 2023 2023. Report No.

895 78. Henry L, Wickham H. rlang: Functions for Base Types and Core R and 'tidyverse'
896 Features. manual. 2024 2024. Report No.

897 79. Wickham H, Vaughan D, Girlich M. tidyr: Tidy Messy Data. manual. 2023 2023.
898 Report No.

899 80. Ooms J. magick: Advanced Graphics and Image-Processing in R. manual. 2023 2023.
900 Report No.

901 81. ImageMagick Studio LLC. ImageMagick. 2023.

902 82. Wickham H, Henry L. purrr: Functional Programming Tools. manual. 2023 2023.
903 Report No.

904 83. Wickham H, Pedersen TL, Seidel D. scales: Scale Functions for Visualization. manual.
905 2023 2023. Report No.

906 84. Merico D, Isserlin R, Stueker O, Emili A, Bader GD. Enrichment map: a network-based
907 method for gene-set enrichment visualization and interpretation. PLoS ONE.
908 2010;5(11):e13984. Epub 20101115. https://doi.org/10.1371/journal.pone.0013984. PubMed
909 PMID: 21085593.

910 85. Shannon P, Markiel A, Ozier O, Baliga NS, Wang JT, Ramage D, et al. Cytoscape: a
911 software environment for integrated models of biomolecular interaction networks. Genome
912 Res. 2003;13(11):2498-504. https://doi.org/10.1101/gr.1239303. PubMed PMID: 14597658.

913 86. Reimand J, Isserlin R, Voisin V, Kucera M, Tannus-Lopes C, Rostamianfar A, et al.
914 Pathway enrichment analysis and visualization of omics data using g:Profiler, GSEA,
915 Cytoscape and EnrichmentMap. Nat Protoc. 2019;14(2):482-517.
916 https://doi.org/10.1038/s41596-018-0103-9. PubMed PMID: 30664679.

917 87. Kucera M, Isserlin R, Arkhangorodsky A, Bader GD. AutoAnnotate: A Cytoscape app
918 for summarizing networks with semantic annotations. F1000Res. 2016;5:1717. Epub
919 20160715. https://doi.org/10.12688/f1000research.9090.1. PubMed PMID: 27830058.

920 88. Morris JH, Apeltsin L, Newman AM, Baumbach J, Wittkop T, Su G, et al.
921 clusterMaker: a multi-algorithm clustering plugin for Cytoscape. BMC Bioinformatics.
922 2011;12:436. Epub 20111109. https://doi.org/10.1186/1471-2105-12-436. PubMed PMID:
923 22070249.

924 89. Oesper L, Merico D, Isserlin R, Bader GD. WordCloud: a Cytoscape plugin to create a
925 visual semantic summary of networks. Source Code Biol Med. 2011;6:7. Epub 20110407.
926 https://doi.org/10.1186/1751-0473-6-7. PubMed PMID: 21473782.

927 90. Becker MY, Rojas I. A graph layout algorithm for drawing metabolic pathways.
928 Bioinformatics. 2001;17(5):461-7. https://doi.org/10.1093/bioinformatics/17.5.461. PubMed
929 PMID: 11331241.

930 91. Magee DA, Taraktsoglou M, Killick KE, Nalpas NC, Browne JA, Park SD, et al. Global
931 gene expression and systems biology analysis of bovine monocyte-derived macrophages in
932 response to in vitro challenge with *Mycobacterium bovis*. PLoS ONE. 2012;7(2):e32034. Epub
933 20120222. https://doi.org/10.1371/journal.pone.0032034. PubMed PMID: 22384131.

934 92. MacHugh DE, Taraktsoglou M, Killick KE, Nalpas NC, Browne JA, E. PSD, et al. Pan-
935 genomic analysis of bovine monocyte-derived macrophage gene expression in response to *in*
936 *vitro* infection with *Mycobacterium avium* subspecies *paratuberculosis*. Vet Res.
937 2012;43(1):25. Epub 20120328. https://doi.org/10.1186/1297-9716-43-25. PubMed PMID:
938 22455317.

939 93. Killick KE, Browne JA, Park SD, Magee DA, Martin I, Meade KG, et al. Genome-wide
940 transcriptional profiling of peripheral blood leukocytes from cattle infected with
941 *Mycobacterium bovis* reveals suppression of host immune genes. BMC Genomics.
942 2011;12:611. Epub 20111219. https://doi.org/10.1186/1471-2164-12-611. PubMed PMID:
943 22182502.

944 94. Ezendam J, Staedtler F, Pennings J, Vandebriel RJ, Pieters R, Harleman JH, et al.
945 Toxicogenomics of subchronic hexachlorobenzene exposure in Brown Norway rats. Environ
946 Health Perspect. 2004;112(7):782-91. https://doi.org/10.1289/ehp.112-1241993. PubMed
947 PMID: 15159207.

948 95. Kriegel H-P, Kröger P, Schubert E, Zimek A, editors. A general framework for
949 increasing the robustness of PCA-based correlation clustering algorithms2008; Berlin,
950 Heidelberg: Springer Berlin Heidelberg.

951 96. McVean G. A genealogical interpretation of principal components analysis. PLoS
952 Genet. 2009;5(10):e1000686. Epub 20091016. https://doi.org/10.1371/journal.pgen.1000686.
953 PubMed PMID: 19834557.

954 97. Novembre J, Stephens M. Interpreting principal component analyses of spatial
955 population genetic variation. Nat Genet. 2008;40(5):646-9. Epub 20080420.
956 https://doi.org/10.1038/ng.139. PubMed PMID: 18425127.

957 98. Lewis SM, Williams A, Eisenbarth SC. Structure and function of the immune system
958 in the spleen. Sci Immunol. 2019;4(33). https://doi.org/10.1126/sciimmunol.aau6085. PubMed
959 PMID: 30824527.

960 99. Buettner M, Bode U. Lymph node dissection – understanding the immunological
961 function of lymph nodes. Clin Exp Immunol. 2012;169(3):205-12.
962 https://doi.org/10.1111/j.1365-2249.2012.04602.x. PubMed PMID: 22861359.

963 100. Jønsson V. Comparison and definition of spleen and lymph node: a phylogenetic
964 analysis. J Theor Biol. 1985;117(4):691-9. https://doi.org/10.1016/s0022-5193(85)80247-2.
965 PubMed PMID: 4094460.

966 101. Dalma-Weiszhausz DD, Warrington J, Tanimoto EY, Miyada CG. The Affymetrix
967 GeneChip platform: an overview. Methods Enzymol. 2006;410:3-28.
968 https://doi.org/10.1016/S0076-6879(06)10001-4. PubMed PMID: 16938544.

969 102. Casey ME, Meade KG, Nalpas NC, Taraktsoglou M, Browne JA, Killick KE, et al.
970 Analysis of the bovine monocyte-derived macrophage response to *Mycobacterium avium*
971 subspecies *paratuberculosis* infection using RNA-seq. Front Immunol. 2015;6:23. Epub
972 20150204. https://doi.org/10.3389/fimmu.2015.00023. PubMed PMID: 25699042.

973 103. McLoughlin KE, Nalpas NC, Rue-Albrecht K, Browne JA, Magee DA, Killick KE, et
974 al. RNA-seq transcriptional profiling of peripheral blood leukocytes from cattle infected with
975 *Mycobacterium bovis*. Front Immunol. 2014;5:396. Epub 20140826.
976 https://doi.org/10.3389/fimmu.2014.00396. PubMed PMID: 25206354.

977 104. Nalpas NC, Park SD, Magee DA, Taraktsoglou M, Browne JA, Conlon KM, et al.
978 Whole-transcriptome, high-throughput RNA sequence analysis of the bovine macrophage
979 response to *Mycobacterium bovis* infection in vitro. BMC Genomics. 2013;14:230. Epub
980 20130408. https://doi.org/10.1186/1471-2164-14-230. PubMed PMID: 23565803.

981 105. Gitau JK, Macharia RW, Mwangi KW, Ongeso N, Murungi E. Gene co-expression
982 network identifies critical genes, pathways and regulatory motifs mediating the progression of
983 Rift Valley Fgorever in *Bos taurus*. Heliyon. 2023;9(7):e18175. Epub 20230714.
984 https://doi.org/10.1016/j.heliyon.2023.e18175. PubMed PMID: 37519716.

985 106. Kuiper JWP, Krause J, Potgeter L, Adrian J, Hauck CR. A genome-wide genetic screen
986 identifies CYRI-B as a negative regulator of CEACAM3-mediated phagocytosis. J Cell Sci.
987 2023;136(11). Epub 20230602. https://doi.org/10.1242/jcs.260771. PubMed PMID:
988 37264948.

989 107. Al Barashdi MA, Ali A, McMullin MF, Mills K. Protein tyrosine phosphatase receptor
990 type C (PTPRC or CD45). J Clin Pathol. 2021;74(9):548-52. Epub 20210526.
991 https://doi.org/10.1136/jclinpath-2020-206927. PubMed PMID: 34039664.

992 108. Goodhead I, Archibald A, Amwayi P, Brass A, Gibson J, Hall N, et al. A
993 comprehensive genetic analysis of candidate genes regulating response to *Trypanosoma*
994 *congolense* infection in mice. PLoS Negl Trop Dis. 2010;4(11):e880. Epub 20101109.
995 https://doi.org/10.1371/journal.pntd.0000880. PubMed PMID: 21085469.

996 109. Noyes HA, Alimohammadian MH, Agaba M, Brass A, Fuchs H, Gailus-Durner V, et
997 al. Mechanisms controlling anaemia in *Trypanosoma congolense* infected mice. PLoS ONE.
998 2009;4(4):e5170. Epub 20090413. https://doi.org/10.1371/journal.pone.0005170. PubMed
999 PMID: 19365556.

1000 110. Guerrero NA, Camacho M, Vila L, Iniguez MA, Chillon-Marinas C, Cuervo H, et al.
1001 Cyclooxygenase-2 and prostaglandin E2 signaling through prostaglandin receptor EP-2 favor
1002 the development of myocarditis during acute *Trypanosoma cruzi* infection. PLoS Negl Trop
1003 Dis. 2015;9(8):e0004025. Epub 20150825. https://doi.org/10.1371/journal.pntd.0004025.
1004 PubMed PMID: 26305786.

1005 111. Pham HTT, Magez S, Choi B, Baatar B, Jung J, Radwanska M. Neutrophil
1006 metalloproteinase driven spleen damage hampers infection control of trypanosomiasis. Nat
1007 Commun. 2023;14(1):5418. Epub 20230905. https://doi.org/10.1038/s41467-023-41089-w.
1008 PubMed PMID: 37669943.

1009 112. Antoine-Moussiaux N, Cornet A, Cornet F, Glineur S, Dermine M, Desmecht D. A
1010 non-cytosolic protein of *Trypanosoma evansi* induces CD45-dependent lymphocyte death.
1011 PLoS ONE. 2009;4(5):e5728. Epub 20090529. https://doi.org/10.1371/journal.pone.0005728.
1012 PubMed PMID: 19478957.

1013 113. Le Coz C, Nguyen DN, Su C, Nolan BE, Albrecht AV, Xhani S, et al. Constrained
1014 chromatin accessibility in PU.1-mutated agammaglobulinemia patients. J Exp Med.
1015 2021;218(7). Epub 20210505. https://doi.org/10.1084/jem.20201750. PubMed PMID:
1016 33951726.

1017 114. Liu W, Rodgers GP. Olfactomedin 4 expression and functions in innate immunity,
1018 inflammation, and cancer. Cancer Metastasis Rev. 2016;35(2):201-12.
1019 https://doi.org/10.1007/s10555-016-9624-2. PubMed PMID: 27178440.

1020 115. Tanioku T, Nishibata M, Tokinaga Y, Konno K, Watanabe M, Hemmi H, et al.
1021 Tmem45b is essential for inflammation- and tissue injury-induced mechanical pain
1022 hypersensitivity. Proc Natl Acad Sci U S A. 2022;119(45):e2121989119. Epub 20221102.
1023 https://doi.org/10.1073/pnas.2121989119. PubMed PMID: 36322717.

1024 116. Röder A, Hüsken S, Hutter MC, Rettie AE, Hanenberg H, Wiek C, et al. Spotlight on
1025 CYP4B1. Int J Mol Sci. 2023;24(3). Epub 20230120. https://doi.org/10.3390/ijms24032038.
1026 PubMed PMID: 36768362.

1027 117. Banworth MJ, Liang Z, Li G. A novel membrane targeting domain mediates the
1028 endosomal or Golgi localization specificity of small GTPases Rab22 and Rab31. J Biol Chem.
1029 2022;298(9):102281. Epub 20220719. https://doi.org/10.1016/j.jbc.2022.102281. PubMed
1030 PMID: 35863437.

1031 118. Jentzsch J, Wunderlich H, Thein M, Bechthold J, Brehm L, Krauss SW, et al.
1032 Microtubule polyglutamylation is an essential regulator of cytoskeletal integrity in
1033 *Trypanosoma brucei*. J Cell Sci. 2024;137(3). Epub 20240212.
1034 https://doi.org/10.1242/jcs.261740. PubMed PMID: 38205672.

1035 119. Kumar R, Ali SA, Singh SK, Bhushan V, Mathur M, Jamwal S, et al. Antimicrobial
1036 peptides in farm animals: an updated review on its diversity, function, modes of action and
1037 therapeutic prospects. Vet Sci. 2020;7(4). Epub 20201218.
1038 https://doi.org/10.3390/vetsci7040206. PubMed PMID: 33352919.

1039 120. Davies D, Meade KG, Herath S, Eckersall PD, Gonzalez D, White JO, et al. Toll-like
1040 receptor and antimicrobial peptide expression in the bovine endometrium. Reprod Biol

1041 Endocrinol. 2008;6:53. Epub 20081118. https://doi.org/10.1186/1477-7827-6-53. PubMed
1042 PMID: 19017375.

1043 121. Tetens J, Friedrich JJ, Hartmann A, Schwerin M, Kalm E, Thaller G. The spatial
1044 expression pattern of antimicrobial peptides across the healthy bovine udder. J Dairy Sci.
1045 2010;93(2):775-83. https://doi.org/10.3168/jds.2009-2729. PubMed PMID: 20105549.

1046 122. Alva-Murillo N, Tellez-Perez AD, Sagrero-Cisneros E, Lopez-Meza JE, Ochoa-
1047 Zarzosa A. Expression of antimicrobial peptides by bovine endothelial cells. Cell Immunol.
1048 2012;280(1):108-12. Epub 20121219. https://doi.org/10.1016/j.cellimm.2012.11.016. PubMed
1049 PMID: 23298865.

1050 123. Krause A, Sillard R, Kleemeier B, Kluver E, Maronde E, Conejo-Garcia JR, et al.
1051 Isolation and biochemical characterization of LEAP-2, a novel blood peptide expressed in the
1052 liver. Protein Sci. 2003;12(1):143-52. https://doi.org/10.1110/ps.0213603. PubMed PMID:
1053 12493837.

1054 124. Whelehan CJ, Barry-Reidy A, Meade KG, Eckersall PD, Chapwanya A, Narciandi F,
1055 et al. Characterisation and expression profile of the bovine cathelicidin gene repertoire in
1056 mammary tissue. BMC Genomics. 2014;15:128. Epub 20140213.
1057 https://doi.org/10.1186/1471-2164-15-128. PubMed PMID: 24524771.

1058 125. McGwire BS, Olson CL, Tack BF, Engman DM. Killing of African trypanosomes by
1059 antimicrobial peptides. J Infect Dis. 2003;188(1):146-52. Epub 20030616.
1060 https://doi.org/10.1086/375747. PubMed PMID: 12825184.

1061 126. Selsted ME, Tang YQ, Morris WL, McGuire PA, Novotny MJ, Smith W, et al.
1062 Purification, primary structures, and antibacterial activities of beta-defensins, a new family of
1063 antimicrobial peptides from bovine neutrophils. J Biol Chem. 1993;268(9):6641-8. PubMed
1064 PMID: 8454635.

1065 127. Regenhard P, Leippe M, Schubert S, Podschun R, Kalm E, Grotzinger J, et al.
1066 Antimicrobial activity of bovine psoriasin. Vet Microbiol. 2009;136(3-4):335-40. Epub
1067 20081206. https://doi.org/10.1016/j.vetmic.2008.12.001. PubMed PMID: 19167844.

1068 128. Uzonna JE, Kaushik RS, Gordon JR, Tabel H. Cytokines and antibody responses during
1069 *Trypanosoma congolense* infections in two inbred mouse strains that differ in resistance.

1070 Parasite Immunol. 1999;21(2):57-71. https://doi.org/10.1046/j.1365-3024.1999.00202.x.
1071 PubMed PMID: 10101716.

1072 129. Soares-Silva M, Diniz FF, Gomes GN, Bahia D. The mitogen-activated protein kinase
1073 (MAPK) pathway: role in immune evasion by trypanosomatids. Front Microbiol. 2016;7:183.
1074 Epub 20160224. https://doi.org/10.3389/fmicb.2016.00183. PubMed PMID: 26941717.

1075 130. Kaur P, Goyal N. Pathogenic role of mitogen activated protein kinases in protozoan
1076 parasites. Biochimie. 2022;193:78-89. Epub 20211024.
1077 https://doi.org/10.1016/j.biochi.2021.10.012. PubMed PMID: 34706251.

1078 131. Kuriakose S, Onyilagha C, Singh R, Olayinka-Adefemi F, Jia P, Uzonna JE. TLR-2
1079 and MyD88-dependent activation of MAPK and STAT proteins regulates proinflammatory
1080 cytokine response and immunity to experimental *Trypanosoma congolense* infection. Front
1081 Immunol. 2019;10:2673. Epub 20191122. https://doi.org/10.3389/fimmu.2019.02673.
1082 PubMed PMID: 31824484.

1083 132. Pays E, Vanhollebeke B, Vanhamme L, Paturiaux-Hanocq F, Nolan DP, Pérez-Morga
1084 D. The trypanolytic factor of human serum. Nat Rev Microbiol. 2006;4(6):477-86.
1085 https://doi.org/10.1038/nrmicro1428.

1086 133. Wellde BT, Chumo DA, Onyango FK, Reardon MJ, Roberts LM, Njogu AR, et al.
1087 *Trypanosoma vivax*: disseminated intravascular coagulation in cattle. Ann Trop Med Parasitol.
1088 1989;83 Suppl 1:177-83. https://doi.org/10.1080/00034983.1989.11812422. PubMed PMID:
1089 2619392.

1090 134. Greenwood BM, Whittle HC. Coagulation studies in Gambian trypanosomiasis. Am J
1091 Trop Med Hyg. 1976;25(3):390-4. https://doi.org/10.4269/ajtmh.1976.25.390. PubMed PMID:
1092 937630.

1093 135. Choudhuri S, Garg NJ. Platelets, macrophages, and thromboinflammation in Chagas
1094 disease. J Inflamm Res. 2022;15:5689-706. Epub 20221004.
1095 https://doi.org/10.2147/JIR.S380896. PubMed PMID: 36217453.

1096 136. Naessens J. Bovine trypanotolerance: A natural ability to prevent severe anaemia and
1097 haemophagocytic syndrome? Int J Parasitol. 2006;36(5):521-8. Epub 20060313.
1098 https://doi.org/10.1016/j.ijpara.2006.02.012. PubMed PMID: 16678182.

1099 137. Stijlemans B, Beschin A, Magez S, Van Ginderachter JA, De Baetselier P. Iron
1100 homeostasis and *Trypanosoma brucei* associated immunopathogenicity development: a
1101 battle/quest for iron. Biomed Res Int. 2015;2015:819389. Epub 20150518.
1102 https://doi.org/10.1155/2015/819389. PubMed PMID: 26090446.

1103 138. Magez S, Schwegmann A, Atkinson R, Claes F, Drennan M, De Baetselier P, et al. The
1104 role of B-cells and IgM antibodies in parasitemia, anemia, and VSG switching in *Trypanosoma*
1105 *brucei*-infected mice. PLoS Pathog. 2008;4(8):e1000122. Epub 20080808.
1106 https://doi.org/10.1371/journal.ppat.1000122. PubMed PMID: 18688274.

1107 139. Gilabert Carbajo C, Cornell LJ, Madbouly Y, Lai Z, Yates PA, Tinti M, et al. Novel
1108 aspects of iron homeostasis in pathogenic bloodstream form *Trypanosoma brucei*. PLoS
1109 Pathog. 2021;17(6):e1009696. Epub 20210623. https://doi.org/10.1371/journal.ppat.1009696.
1110 PubMed PMID: 34161395.

1111 140. Taylor MC, Kelly JM. Iron metabolism in trypanosomatids, and its crucial role in
1112 infection. Parasitology. 2010;137(6):899-917. Epub 20100215.
1113 https://doi.org/10.1017/S0031182009991880. PubMed PMID: 20152063.

1114 141. Dick CF, Alcantara CL, Carvalho-Kelly LF, Lacerda-Abreu MA, Cunha ESNL, Meyer-
1115 Fernandes JR, et al. Iron uptake controls *Trypanosoma cruzi* metabolic shift and cell
1116 proliferation. Antioxidants (Basel). 2023;12(5). Epub 20230422.
1117 https://doi.org/10.3390/antiox12050984. PubMed PMID: 37237850.

1118 142. Basu S, Horakova E, Lukes J. Iron-associated biology of *Trypanosoma brucei*. Biochim
1119 Biophys Acta. 2016;1860(2):363-70. Epub 20151030.
1120 https://doi.org/10.1016/j.bbagen.2015.10.027. PubMed PMID: 26523873.

1121 143. Steverding D. Bloodstream forms of *Trypanosoma brucei* require only small amounts
1122 of iron for growth. Parasitol Res. 1998;84(1):59-62. https://doi.org/10.1007/s004360050357.
1123 PubMed PMID: 9491428.

1124 144. Stijlemans B, Vankrunkelsven A, Brys L, Magez S, De Baetselier P. Role of iron
1125 homeostasis in trypanosomiasis-associated anemia. Immunobiology. 2008;213(9-10):823-35.
1126 Epub 20080907. https://doi.org/10.1016/j.imbio.2008.07.023. PubMed PMID: 18926297.

1127 145. Stijlemans B, Vankrunkelsven A, Caljon G, Bockstal V, Guilliams M, Bosschaerts T,
1128 et al. The central role of macrophages in trypanosomiasis-associated anemia: rationale for
1129 therapeutical approaches. Endocr Metab Immune Disord Drug Targets. 2010;10(1):71-82.
1130 https://doi.org/10.2174/187153010790827966. PubMed PMID: 20158497.

1131 146. Naessens J, Leak SG, Kennedy DJ, Kemp SJ, Teale AJ. Responses of bovine chimaeras
1132 combining trypanosomosis resistant and susceptible genotypes to experimental infection with
1133 Trypanosoma congolense. Vet Parasitol. 2003;111(2-3):125-42.
1134 https://doi.org/10.1016/s0304-4017(02)00360-6. PubMed PMID: 12531289.

1135 147. Donovan A, Lima CA, Pinkus JL, Pinkus GS, Zon LI, Robine S, et al. The iron exporter
1136 ferroportin/Slc40a1 is essential for iron homeostasis. Cell Metab. 2005;1(3):191-200.
1137 https://doi.org/10.1016/j.cmet.2005.01.003. PubMed PMID: 16054062.

1138 148. Holder A, Garty R, Elder C, Mesnard P, Laquerbe C, Bartens MC, et al. Analysis of
1139 genetic variation in the bovine *SLC11A1* gene, its influence on the expression of *NRAMP1* and
1140 potential association with resistance to bovine tuberculosis. Front Microbiol. 2020;11:1420.
1141 Epub 20200630. https://doi.org/10.3389/fmicb.2020.01420. PubMed PMID: 32714308.

1142 149. Archer NS, Nassif NT, O'Brien BA. Genetic variants of SLC11A1 are associated with
1143 both autoimmune and infectious diseases: systematic review and meta-analysis. Genes Immun.
1144 2015;16(4):275-83. Epub 20150409. https://doi.org/10.1038/gene.2015.8. PubMed PMID:
1145 25856512.

1146

1147 # Supporting information captions

1148 **Table S1.** Contrast ID, contrast type, tissue, days post infection (dpi), and formula for each of
1149 the 64 contrasts.

1150 **Table S2.** Differential expression analysis results including the probe ID, gene ID, $\log_2$ fold
1151 change, and $P_{adj.}$ for each of the 64 contrasts.

1152 **Table S3.** Tissue, days post infection (dpi), and the top 10 most significant genes with
1153 increased and decreased expression with valid gene symbols for the direct contrasts.

1154 **Table S4.** Tissue, days post infection (dpi), and the top 10 most significant genes with
1155 increased and decreased expression with valid gene symbols for the N'Dama contrasts.

1156 **Table S5.** Tissue, days post infection (dpi), and the top 10 most significant genes with
1157 increased and decreased expression with valid gene symbols for the Boran contrasts.

1158 **Fig S1.** Boxplots showing the $\log_2$ expression intensity of the probe sets for each sample of
1159 the **A.** raw and **B.** normalised data after quality control filtering separated into NDAM and
1160 BORA populations and coloured according to tissue. The position along the horizontal axis
1161 indicates the days post infection. Outlier probe sets are shown as grey dots.

1162 **Fig S2. A.** Principal component analysis (PCA) of the microarray data set with samples
1163 coloured according to days post infection (dpi) with the outer colour representing the tissue
1164 and shape indicating the population showing the first and third principal components (PC1
1165 and PC3), and **B.** bar chart of proportion of variance of the top ten PCs.

1166 **Fig S3. A.** Principal component analysis (PCA) of the microarray data set with samples
1167 coloured according to days post infection (dpi) with the outer colour representing the tissue
1168 and shape indicating the population showing the first and fourth principal components (PC1
1169 and PC4), and **B.** bar chart of proportion of variance of the top ten PCs.

1170 **Fig S4. A.** Principal component analysis (PCA) of the microarray data set with samples
1171 coloured according to tissue and shape indicating the population showing the first and fifth
1172 principal components (PC1 and PC5), and **B.** bar chart of proportion of variance of the top ten
1173 PCs.

1174 **Fig S5.** Bar chart showing the numbers of significantly differentially expressed genes for the
1175 RESP contrasts. The extent of the bar above and below 0 on the vertical axis indicates the
1176 numbers of significantly differentially expressed genes (DEGs) with increased and decreased
1177 expression, respectively. The position on the horizontal indicates the number of days post
1178 infection (dpi) and the colour of the bars represents the tissue.

1179 **Fig S6.** Bar chart showing the numbers of significantly differentially expressed genes for the
1180 DIRE contrasts. The extent of the bar above and below 0 on the vertical axis indicates the
1181 numbers of significantly differentially expressed genes (DEGs) with increased and decreased
1182 expression, respectively. The position on the horizontal indicates the number of days post
1183 infection (dpi) and the colour of the bars represents the tissue.

1184 **Fig S7.** Bar chart showing the numbers of significantly differentially expressed genes for the
1185 NDAM contrasts. The extent of the bar above and below 0 on the vertical axis indicates the
1186 numbers of significantly differentially expressed genes (DEGs) with increased and decreased
1187 expression, respectively. The position on the horizontal indicates the number of days post
1188 infection (dpi) and the colour of the bars represents the tissue.

1189 **Fig S8.** Bar chart showing the numbers of significantly differentially expressed genes for the
1190 BORA contrasts. The extent of the bar above and below 0 on the vertical axis indicates the
1191 numbers of significantly differentially expressed genes (DEGs) with increased and decreased
1192 expression, respectively. The position on the horizontal indicates the number of days post
1193 infection (dpi) and the colour of the bars represents the tissue.

1194 **Fig S9.** UpSet plot showing the top 20 intersections among all 64 contrasts. The horizontal
1195 bars indicate the total number of significant differentially expressed genes (DEGs) for each
1196 contrast while the vertical bars indicate the number of significant DEGs in common between
1197 the contrasts annotated with black dots connected by lines in the intersection matrix. The
1198 background colour of the stripes in the intersection matrix and horizontal bars represents the
1199 tissue. The colour of the bars represents the contrast type with black bars indicating an
1200 overlap between different contrast types. The outline colour of the bars also represents the
1201 tissue with no outline representing an overlap between different tissues.

1202 **Fig S10.** UpSet plot showing the top 20 intersections among the RESP contrasts. The horizontal
1203 bars indicate the total number of significant differentially expressed genes (DEGs) for each
1204 contrast while the vertical bars indicate the number of significant DEGs in common between
1205 the contrasts annotated with black dots connected by lines in the intersection matrix. The
1206 background colour of the stripes in the intersection matrix and horizontal bars represents the
1207 tissue. The colour of the bars represents the days post infection (dpi) with black bars
1208 indicating an overlap between different timepoints. The outline colour of the bars also
1209 represents the tissue with no outline representing an overlap between different tissues.

1210 **Fig S11.** UpSet plot showing the top 20 intersections among the DIRE contrasts. The horizontal
1211 bars indicate the total number of significant differentially expressed genes (DEGs) for each
1212 contrast while the vertical bars indicate the number of significant DEGs in common between
1213 the contrasts annotated with black dots connected by lines in the intersection matrix. The
1214 background colour of the stripes in the intersection matrix and horizontal bars represents the
1215 tissue. The colour of the bars represents the days post infection (dpi) with black bars

1216 indicating an overlap between different timepoints. The outline colour of the bars also
1217 represents the tissue with no outline representing an overlap between different tissues.

1218 **Fig S12.** UpSet plot showing the top 20 intersections among the NDAM contrasts. The
1219 horizontal bars indicate the total number of significant differentially expressed genes (DEGs)
1220 for each contrast while the vertical bars indicate the number of significant DEGs in common
1221 between the contrasts annotated with black dots connected by lines in the intersection
1222 matrix. The background colour of the stripes in the intersection matrix and horizontal bars
1223 represents the tissue. The colour of the bars represents the days post infection (dpi) with
1224 black bars indicating an overlap between different timepoints. The outline colour of the bars
1225 also represents the tissue with no outline representing an overlap between different tissues.

1226 **Fig S13.** UpSet plot showing the top 20 intersections among the BORA contrasts. The
1227 horizontal bars indicate the total number of significant differentially expressed genes (DEGs)
1228 for each contrast while the vertical bars indicate the number of significant DEGs in common
1229 between the contrasts annotated with black dots connected by lines in the intersection
1230 matrix. The background colour of the stripes in the intersection matrix and horizontal bars
1231 represents the tissue. The colour of the bars represents the days post infection (dpi) with
1232 black bars indicating an overlap between different timepoints. The outline colour of the bars
1233 also represents the tissue with no outline representing an overlap between different tissues.

1234 **Fig S14.** Volcano plot showing the results of the RESP contrast for the peripheral blood
1235 mononuclear cell (PBMC) samples at 14 days post infection (dpi). Each data point represents
1236 a gene with the position on the *x*- and *y*-axes indicating the $\log_2$ fold change and $-\log_{10}P_{adj.}$,
1237 respectively. Genes above the horizontal dashed line are significantly differentially expressed
1238 with the colours representing the change in expression. The top 10 most significant genes for
1239 increased and decreased expression with gene symbols are labelled.

1240 **Fig S15.** Volcano plot showing the results of the RESP contrast for the peripheral blood
1241 mononuclear cell (PBMC) samples at 25 days post infection (dpi). Each data point represents
1242 a gene with the position on the *x*- and *y*-axes indicating the $\log_2$ fold change and $-\log_{10}P_{adj.}$,
1243 respectively. Genes above the horizontal dashed line are significantly differentially expressed
1244 with the colours representing the change in expression. The top 10 most significant genes for
1245 increased and decreased expression with gene symbols are labelled.

1246 **Fig S16.** Volcano plot showing the results of the RESP contrast for the liver samples at 12 days
1247 post infection (dpi). Each data point represents a gene with the position on the *x*- and *y*-axes
1248 indicating the $\log_2$ fold change and $-\log_{10}P_{adj.}$, respectively. Genes above the horizontal dashed
1249 line are significantly differentially expressed with the colours representing the change in
1250 expression. The top 10 most significant genes for increased and decreased expression with
1251 gene symbols are labelled.

1252 **Fig S17.** Volcano plot showing the results of the RESP contrast for the liver samples at 15 days
1253 post infection (dpi). Each data point represents a gene with the position on the *x*- and *y*-axes
1254 indicating the $\log_2$ fold change and $-\log_{10}P_{adj.}$, respectively. Genes above the horizontal dashed
1255 line are significantly differentially expressed with the colours representing the change in
1256 expression. The top 10 most significant genes for increased and decreased expression with
1257 gene symbols are labelled.

1258 **Fig S18.** Volcano plot showing the results of the RESP contrast for the liver samples at 18 days
1259 post infection (dpi). Each data point represents a gene with the position on the *x*- and *y*-axes
1260 indicating the $\log_2$ fold change and $-\log_{10}P_{adj.}$, respectively. Genes above the horizontal dashed
1261 line are significantly differentially expressed with the colours representing the change in
1262 expression. The top 10 most significant genes for increased and decreased expression with
1263 gene symbols are labelled.

1264 **Fig S19.** Volcano plot showing the results of the RESP contrast for the liver samples at 21 days
1265 post infection (dpi). Each data point represents a gene with the position on the *x*- and *y*-axes
1266 indicating the $\log_2$ fold change and $-\log_{10}P_{adj.}$, respectively. Genes above the horizontal dashed
1267 line are significantly differentially expressed with the colours representing the change in
1268 expression. The top 10 most significant genes for increased and decreased expression with
1269 gene symbols are labelled.

1270 **Fig S20.** Volcano plot showing the results of the RESP contrast for the liver samples at 26 days
1271 post infection (dpi). Each data point represents a gene with the position on the *x*- and *y*-axes
1272 indicating the $\log_2$ fold change and $-\log_{10}P_{adj.}$, respectively. Genes above the horizontal dashed
1273 line are significantly differentially expressed with the colours representing the change in
1274 expression. The top 10 most significant genes for increased and decreased expression with
1275 gene symbols are labelled.

1276 **Fig S21.** Volcano plot showing the results of the RESP contrast for the liver samples at 29 days
1277 post infection (dpi). Each data point represents a gene with the position on the *x*- and *y*-axes
1278 indicating the $\log_2$ fold change and $-\log_{10}P_{adj.}$, respectively. Genes above the horizontal dashed
1279 line are significantly differentially expressed with the colours representing the change in
1280 expression. The top 10 most significant genes for increased and decreased expression with
1281 gene symbols are labelled.

1282 **Fig S22.** Volcano plot showing the results of the RESP contrast for the liver samples at 32 days
1283 post infection (dpi). Each data point represents a gene with the position on the *x*- and *y*-axes
1284 indicating the $\log_2$ fold change and $-\log_{10}P_{adj.}$, respectively. Genes above the horizontal dashed
1285 line are significantly differentially expressed with the colours representing the change in
1286 expression. The top 10 most significant genes for increased and decreased expression with
1287 gene symbols are labelled.

1288 **Fig S23.** Volcano plot showing the results of the RESP contrast for the liver samples at 35 days
1289 post infection (dpi). Each data point represents a gene with the position on the *x*- and *y*-axes
1290 indicating the $\log_2$ fold change and $-\log_{10}P_{adj.}$, respectively. Genes above the horizontal dashed
1291 line are significantly differentially expressed with the colours representing the change in
1292 expression. The top 10 most significant genes for increased and decreased expression with
1293 gene symbols are labelled.

1294 **Fig S24.** Volcano plot showing the results of the RESP contrast for the lymph node samples at
1295 21 days post infection (dpi). Each data point represents a gene with the position on the *x*- and
1296 *y*-axes indicating the $\log_2$ fold change and $-\log_{10}P_{adj.}$, respectively. Genes above the horizontal
1297 dashed line are significantly differentially expressed with the colours representing the change
1298 in expression. The top 10 most significant genes for increased and decreased expression with
1299 gene symbols are labelled.

1300 **Fig S25.** Volcano plot showing the results of the RESP contrast for the lymph node samples at
1301 35 days post infection (dpi). Each data point represents a gene with the position on the *x*- and
1302 *y*-axes indicating the $\log_2$ fold change and $-\log_{10}P_{adj.}$, respectively. Genes above the horizontal
1303 dashed line are significantly differentially expressed with the colours representing the change
1304 in expression. The top 10 most significant genes for increased and decreased expression with
1305 gene symbols are labelled.

1306 **Fig S26.** Volcano plot showing the results of the RESP contrast for the spleen samples at 21
1307 days post infection (dpi). Each data point represents a gene with the position on the *x*- and *y*-
1308 axes indicating the $\log_2$ fold change and $-\log_{10}P_{adj.}$, respectively. Genes above the horizontal
1309 dashed line are significantly differentially expressed with the colours representing the change
1310 in expression. The top 10 most significant genes for increased and decreased expression with
1311 gene symbols are labelled.

1312 **Fig S27.** Volcano plot showing the results of the RESP contrast for the spleen samples at 35
1313 days post infection (dpi). Each data point represents a gene with the position on the *x*- and *y*-
1314 axes indicating the $\log_2$ fold change and $-\log_{10}P_{adj.}$, respectively. Genes above the horizontal
1315 dashed line are significantly differentially expressed with the colours representing the change
1316 in expression. The top 10 most significant genes for increased and decreased expression with
1317 gene symbols are labelled.**Fig S28.** g:Profiler functional enrichment of significantly
1318 differentially expressed genes (DEGs) in the peripheral blood mononuclear cell (PBMC)
1319 sample RESP contrasts. Each circle represents a significantly enriched GO term with the size
1320 indicating the ratio of the intersection between the term and the DEGs. The vertical axis
1321 shows the $-\log_{10}P_{adj.}$ value and the vertical panels and colours indicate the direction of change
1322 in expression. The horizontal panels indicate the source of the term and the position within
1323 the panels groups terms from the same GO subtree. The top driver GO terms (up to a
1324 maximum of 10) are indicated with a black outline and label.

1325 **Fig S29.** g:Profiler functional enrichment of significantly differentially expressed genes (DEGs)
1326 in the liver sample RESP contrasts. Each circle represents a significantly enriched GO term
1327 with the size indicating the ratio of the intersection between the term and the DEGs. The
1328 vertical axis shows the $-\log_{10}P_{adj.}$ value and the vertical panels and colours indicate the
1329 direction of change in expression. The horizontal panels indicate the source of the term and
1330 the position within the panels groups terms from the same GO subtree. The top driver GO
1331 terms (up to a maximum of 10) are indicated with a black outline and label.

1332 **Fig S30.** g:Profiler functional enrichment of significantly differentially expressed genes (DEGs)
1333 in the lymph node sample RESP contrasts. Each circle represents a significantly enriched GO
1334 term with the size indicating the ratio of the intersection between the term and the DEGs.
1335 The vertical axis shows the $-\log_{10}P_{adj.}$ value and the vertical panels and colours indicate the
1336 direction of change in expression. The horizontal panels indicate the source of the term and
1337 the position within the panels groups terms from the same GO subtree. The top driver GO
1338 terms (up to a maximum of 10) are indicated with a black outline and label.

1339 **Fig S31.** g:Profiler functional enrichment of significantly differentially expressed genes (DEGs)
1340 in the spleen sample RESP contrasts. Each circle represents a significantly enriched GO term
1341 with the size indicating the ratio of the intersection between the term and the DEGs. The
1342 vertical axis shows the $-\log_{10}P_{adj.}$ value and the vertical panels and colours indicate the
1343 direction of change in expression. The horizontal panels indicate the source of the term and
1344 the position within the panels groups terms from the same GO subtree. The top driver GO
1345 terms (up to a maximum of 10) are indicated with a black outline and label.

1346 **Fig S32.** EnrichmentMap network of significantly enriched GO terms identified from g:Profiler
1347 functional enrichment of significant differentially expressed genes (DEGs) for the DIRE
1348 contrasts.Each node represents a GO term with the colour of the node representing the tissue
1349 and the size representing the number of genes in the GO term. The edges indicate overlap
1350 between the GO terms with the width of the edges representing the similarity coefficient for
1351 the connected GO terms. The GO terms are clustered by AutoAnotate with the background
1352 colour of the clusters representing the direction of expression. The clusters are labelled with
1353 the size of the label scaling with the number of GO terms in the cluster.

1354 **Fig S33.** EnrichmentMap network of significantly enriched GO terms identified from g:Profiler
1355 functional enrichment of significant differentially expressed genes (DEGs) for the NDAM
1356 contrasts. Each node represents a GO term with the colour of the node representing the tissue
1357 and the size representing the number of genes in the GO term. The edges indicate overlap
1358 between the GO terms with the width of the edges representing the similarity coefficient for
1359 the connected GO terms. The GO terms are clustered by AutoAnotate with the background
1360 colour of the clusters representing the direction of expression. The clusters are labelled with
1361 the size of the label scaling with the number of GO terms in the cluster.

1362 **Fig S34.** EnrichmentMap network of significantly enriched GO terms identified from g:Profiler
1363 functional enrichment of significant differentially expressed genes (DEGs) for the BORA
1364 contrasts. Each node represents a GO term with the colour of the node representing the tissue
1365 and the size representing the number of genes in the GO term. The edges indicate overlap
1366 between the GO terms with the width of the edges representing the similarity coefficient for
1367 the connected GO terms. The GO terms are clustered by AutoAnotate with the background
1368 colour of the clusters representing the direction of expression. The clusters are labelled with
1369 the size of the label scaling with the number of GO terms in the cluster.